Electronic Supplementary Material (ESI) for Journal of Materials Chemistry C.

Electronic Supplementary Information

Supramolecular Polymerization of Chiral Platinum(II) Complexes: Transformable Nanoassemblies and Their Amplified Circularly Polarized Luminescence

Xiaolin Zhu,*† Zhen Wang,† Yihui Jia, Fang Yang, Youzhi Zhang, Shirui Zhao, Xiaoming He*

*To whom correspondence should be addressed

Key Laboratory of Applied Surface and Colloid Chemistry (Ministry of Education), School of Chemistry and Chemical Engineering, Shaanxi Normal University, Xi'an 710119, P.R. China

*Corresponding Author Email: xiaolinchem@snnu.edu.cn (Xiaolin Zhu); xmhe@snnu.edu.cn (Xiaoming He)

Materials and Methods

Materials. All the chemical reagents were purchased from commercial sources (Aldrich, Alfa Aesar, Energy Chemical and Adamas) and were used as received unless otherwise noted.

Characterizations. ^{1}H NMR and ^{13}C NMR spectra were recorded on a 600 MHz BRUKER spectrometer at room temperature using tetramethylsilane (TMS) as the internal standard. High-resolution mass spectrometry (HRMS) data were collected on a Bruker maxis UHR-TOF mass spectrometer in ESI positive mode. Fourier transform infrared (FT-IR) measurements were carried out using a Bruker Tensor27 spectrophotometer. PXRD patterns were recorded on a Bruker D8 Advance instrument. X-ray single crystal diffraction data were collected on a Nonius Kappa CCD diffractometer, using Mo Kα radiation (λ) 0.71073 Å (graphite monochromator). UV-vis spectra were recorded on an Agilent Technologies Cary 3500 spectrometer. Emission spectra and the absolute quantum yields were recorded on a Horiba FluoroMax Plus spectrofluorometer. CD experiments were performed using a Chirascan CD spectrometer. CPL spectra and subsequently derived glum values were recorded using an OLIS CPL Solo spectrofluorometer and the globalworks software suite. PL lifetimes were measured using an FLS1000 fluorescence spectrometer (Edinburgh) at room temperature. Scanning electron microscopy (SEM) was performed using a Hitachi SU8220. Transmission electron microscopy (TEM) micrographs were obtained using a Hitachi TEM HT 7800 operating at 80 kV acceleration voltage. The high-angle annular dark-field (HAADF) imaging and EDX images were obtained using an FEI Titan cubed Themis G2 300 microscope operated at 300 kV and equipped with a probe aberration corrector and a monochromator. The samples were dropped onto a carbon-coated copper grid and dried. Atomic force microscopy (AFM) experiments were performed on an Asylum Research Cypher VRS (Oxford instruments) atomic force microscope equipped with a Scan Asyst-HR fast scanning module and a Scan Asyst Air-HR probe (tip radius, 2 nm), utilizing peak force feedback control. The $CHCl_3$-MCH mixture solutions of the complexes were drop-casted onto the mica sheets for the AFM sampling preparation.

Experimental section

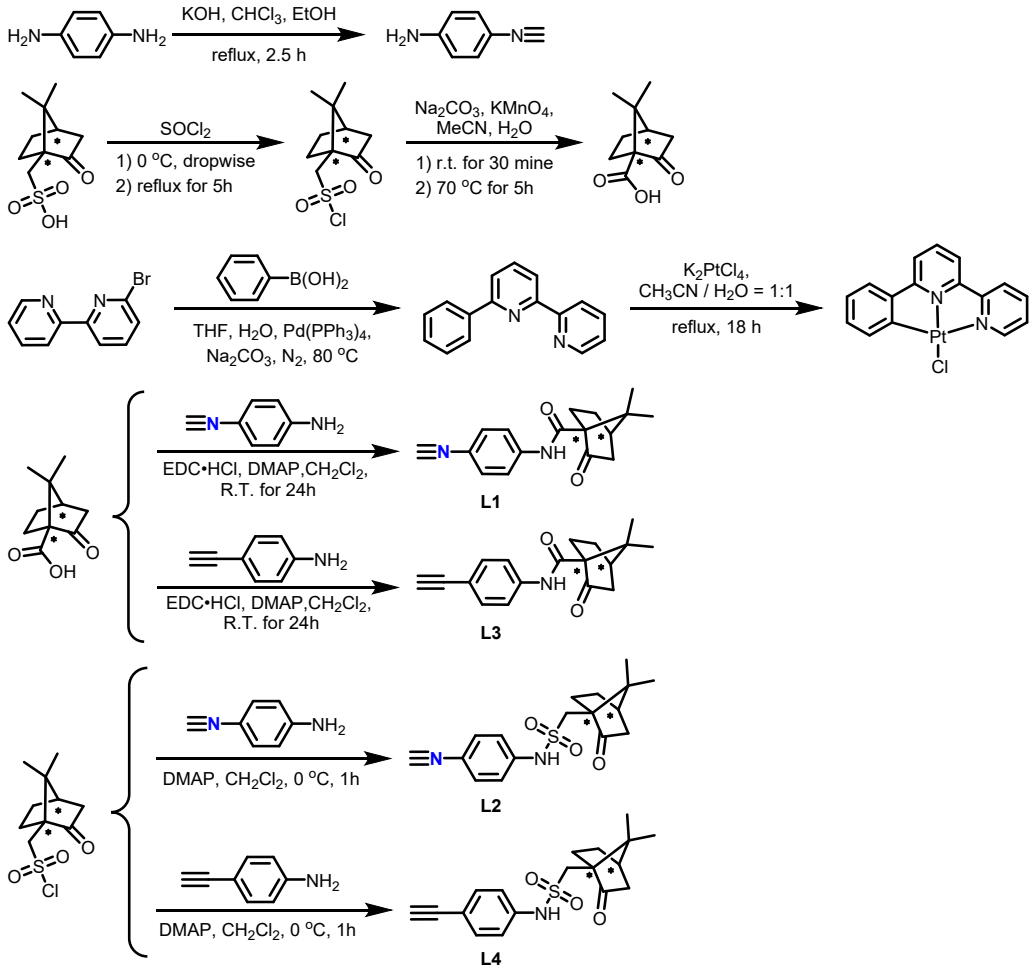

Scheme S1. Synthetic route of ligands **L1** to **L4**.

Synthesis of key precursors. 4-Isocyanobenzenamine[1], 6-phenyl-2,2'-bipyridine[2], chloro(6-phenyl-2,2'-bipyridine)platinum[3], 10-camphorsulfonyl chloride[4], and ketopinic acid[4] were synthesized according to the previously reported procedures.

Synthesis of ligands L1. To a 250 mL Schlenk flask, ketopinic acid (1.0 mmol, 1.0 equiv.), 4-isocyanobenzenamine (1.1 mmol, 1.1 equiv.), EDC·HCl (1-Ethyl-3-(3-dimethylaminopropyl) carbodiimide hydrochloride, 1.1 mmol, 1.1 equiv.), DMAP (4-Dimethyl-aminopyridine, 0.7 mmol, 0.7 equiv.) and dry CH_2Cl_2 (60 mL) were added. Then the mixture was stirred at R.T. for 24 h under N_2. The reaction mixture was then quenched by adding 50 mL water. The mixture was extracted with CH_2Cl_2 (3×50 mL), the combined organic layer was washed with 1M aqueous HCl (20 mL) and brine (200 mL). After drying over anhydrous Na_2SO_4 and filtration, the solvent was evaporated under vacuum to give the product as a pale-yellow solid.

D-L1. Yield 85%. ^{1}H NMR (600 MHz, DMSO): δ 9.46 (s, 1H), 7.79 (d, J = 8.6 Hz, 2H), 7.51 (d, J = 8.6 Hz, 2H), 2.54 (dt, J_1 = 18.5 Hz, J_2 = 3.8 Hz, 1H), 2.34 - 2.27 (m, 1H), 2.08 - 1.91 (m, 4H), 1.48 - 1.41 (m, 1H), 1.11 (s, 3H), 1.10 (s, 3H). ^{13}C NMR (151 MHz, DMSO): δ 212.88, 167.69, 139.77, 126.79, 120.54, 67.21, 48.94, 43.25, 43.19, 26.71, 26.27, 20.73, 19.93. HRMS (ESI) calcd for $[C_{17}H_{18}N_2NaO_2]^+$, 305.1260; found, 305.1255.

L-L1. Yield 84%. The characterization data of **L-L1** was in consistent with those of **D-L1**.

Synthesis of ligand L-2. To a 100 ml Schlenk flask equipped was added 4-isocyanoaniline (7.2 mmol, 0.9 equiv.), 1-(3-dimethylaminopropyl)-3-ethylcarbodiimide hydrochloride (8.8 mmol, 1.1 equiv.) and dry CH_2Cl_2 (30 mL) under N_2. Then the mixture was stirred at 0 ℃ for 15 min before adding the solution of 10-camphorsulfonyl chloride (7.98 mmol, 1.0 equiv.) in CH_2Cl_2 (8 mL). Then the final solution was stirred at 0 ℃ for 1 h. Subsequently 35 mL EtOAc was added to precipitate triethylammonium hydrochloride. The reaction mixture was then quenched by adding water, 1 M aqueous HCl and brine. After drying over anhydrous Na_2SO_4, the solvent was evaporated under vacuum. The product was obtained as a pale-yellow solid.

D-L2. Yield 88%. ^{1}H NMR (600 MHz, DMSO): δ 10.32 (s, 1H), 7.56 (d, J = 8.8 Hz, 2H), 7.30 (d, J = 8.8 Hz, 2H), 3.43 (d, J = 15.0 Hz, 1H), 3.07 (d, J = 15.0 Hz, 1H), 2.37 - 2.29 (m, 2H), 2.06 (t, J = 4.6 Hz, 1H), 1.98 - 1.90 (m, 2H), 1.58 - 1.52 (m, 1H), 1.45 - 1.38 (m, 1H), 0.99 (s, 3H), 0.76 (s, 3H). ^{13}C NMR (151 MHz, DMSO): δ 213.98, 139.72, 127.59, 118.82, 57.74, 48.17, 47.66, 42.02, 41.93, 26.17, 24.62, 19.27. HRMS (ESI) calcd for $[C_{17}H_{20}N_2NaO_3S]^+$, 355.1087; found, 355.1077.

L-L2. Yield 46%. The characterization data of **L-L2** was in consistent with those of **D-L2**.

Synthesis of ligands L3. The procedures were similar to that of complex **L1**, except that 4-isocyanobenzenamine was replaced by 4-ethynylaniline (1.1 mmol, 1.1 equiv.) to give the product a pale-yellow solid.

D-L3. Yield 85%. ^{1}H NMR (600 MHz, $CDCl_3$): δ 9.81 (s, 1H; NH), 7.59 (d, J = 8.6 Hz, 2H; C_6H_4), 7.45 (d, J = 7.08 Hz, 2H; C_6H_4), 3.04 (s, 1H; CH_2), 2.63 - 2.53 (m, 2H; CH_2), 2.29 - 1.98 (m, 3H; CH_2), 1.76 - 1.66 (m, 1H; CH_2), 1.53 - 1.44 (m, 1H; CH_2), 1.34 (s, 3H; CH_3), 1.03 (s, 3H; CH_3). ^{13}C NMR (151 MHz, $CDCl_3$): δ 218.01, 167.80, 138.48, 133.00, 119.92, 117.67, 83.67, 64.95, 50.86, 43.88, 43.33, 29.23, 28.04, 21.26, 20.54. HRMS (ESI) calcd for $[C_{18}H_{19}NNaO_2]^+$, 304.1308; found, 304.1300.

L-L3. Yield 86%. The characterization data of **L-L3** was consistent with those of **D-L3**.

Synthesis of ligand L4. The procedures were similar to that of complex **L2**, except that 4-isocyanobenzenamine was replaced by 4-ethynylaniline (7.2 mmol, 0.9 equiv.) to give the product as pale-yellow solid.

D-L4. Yield 78%. ^{1}H NMR (600 MHz, $CDCl_3$): δ 7.88 (s, 1H), 7.46 (d, J = 7.2 Hz, 2H), 7.25 (d, J = 8.5 Hz, 2H), 3.31 (d, J = 15.3 Hz, 1H), 3.07 (s, 1H), 2.89 (d, J = 15.3 Hz, 1H), 2.48 - 2.41 (m, 1H), 2.21 - 2.13 (m, 2H), 2.12 - 2.01 (m, 2H), 1.97 (d, J = 18.8 Hz, 1H), 1.51 - 1.46 (m, 1H), 0.96 (s, 3H), 0.84 (s, 3H). ^{13}C NMR (151 MHz, DMSO): δ 217.71, 138.27, 133.47, 121.48, 119.12, 83.13, 77.56, 59.87, 49.64, 49.34, 43.23, 42.96, 27.80, 27.20, 20.01, 19.45. HRMS (ESI) calcd for $[C_{18}H_{21}NNaO_3S]^+$, 354.1134; found, 354.1132.

L-L4. Yield 75%. The characterization data of **L-L4** was in consistent with those of **D-L4**.

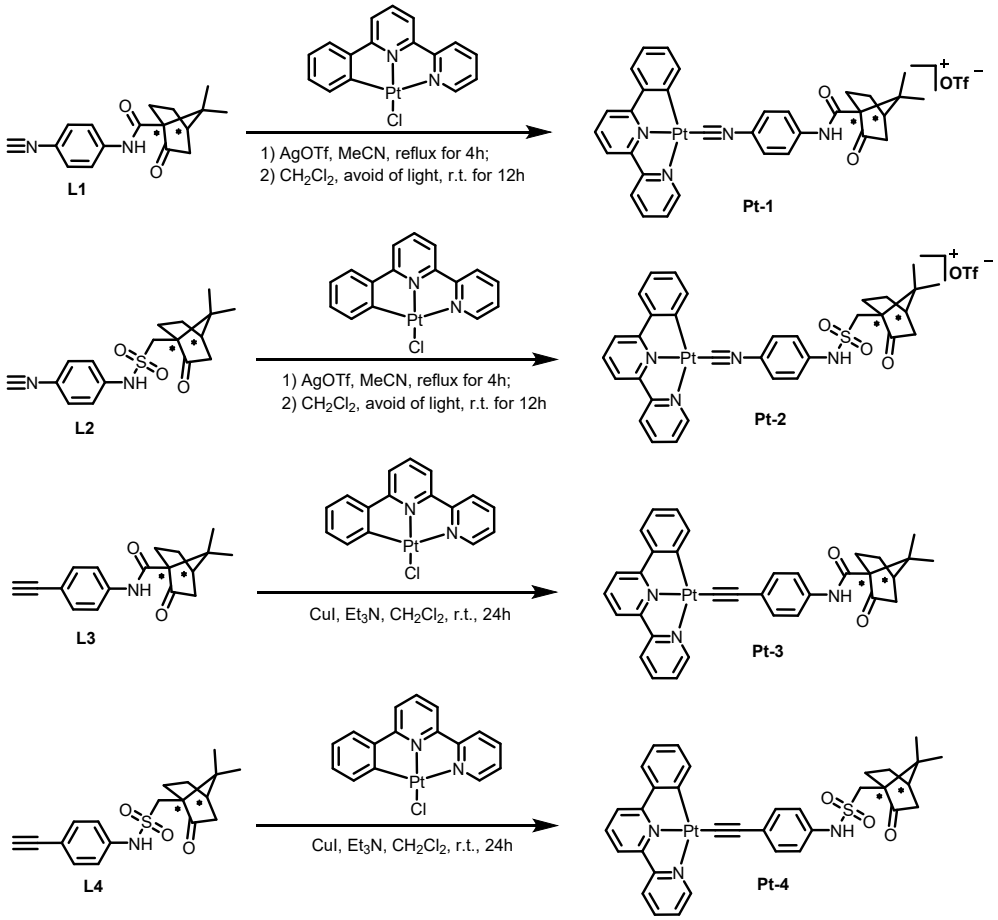

Scheme S2. Synthetic route of **Pt-1** to **Pt-4**.

Synthesis of Pt-1. A suspension of [Pt(C^N^N) Cl] (0.1 mmol, 1.0 equiv.) and AgOTf (0.105 mmol, 1.05 equiv.) in acetonitrile (10 mL) was refluxed for 4 h. After cooled to R.T., and the corresponding CH_2Cl_2 solution (2 mL) of chiral isocyanide ligand **L1** (0.1 mmol, 1.0 equiv.) was

added. After the mixture was further stirred at R.T. for 12 h in darkness, the solution was filtered through celite, and the celite pad was washed with CH_2Cl_2. The product was obtained by the evaporation of solvents and washed with H_2O and Et_2O, respectively. The product was afforded as dark-red solid.

D-Pt-1. Yield 60%. ^{1}H NMR (600 MHz, CD_3CN): δ 9.46 (s, 1H), 8.18 (d, J = 5.0 Hz, 1H), 7.91 (t, J = 7.7 Hz, 1H), 7.70 (t, J = 7.9 Hz, 3H), 7.65 (t, J = 7.8 Hz, 1H), 7.38 (d, J = 7.7 Hz, 1H), 7.33 (t, J = 3.84 Hz, 1H), 7.30 (d, J = 8.8 Hz, 2H), 7.24 (d, J = 8.1 Hz, 1H), 6.94 (d, J = 7.7 Hz, 1H), 6.81 (t, J = 8.5 Hz, 1H), 6.74 (t, J = 5.8 Hz, 1H), 6.68 (d, J = 7.3 Hz, 1H), 2.62 (dt, J_1 = 18.2 Hz, J_2 = 3.9 Hz, 1H), 2.49-2.45 (m, 1H), 2.21-2.15 (m, 3H), 2.07 (d, J = 18.2 Hz, 2H), 1.84-1.77 (m, 1H), 1.56-1.49 (m, 1H), 1.26 (s, 3H), 1.07 (s, 3H). ^{13}C NMR (151 MHz, CD_3CN): δ 216.92, 168.95, 153.32, 143.42, 141.84, 141.16, 138.53, 137.14, 133.00, 129.78, 128.38, 126.69, 125.00, 121.34, 120.87, 120.45, 65.90, 51.43, 43.99, 43.85, 28.92, 27.62, 20.70, 20.61. HRMS (ESI) calcd for $[C_{33}H_{29}N_4O_2Pt]^+$, 708.1936; found, 708.1924. Elemental analysis calcd (%) for $C_{34}H_{29}F_3N_4O_5PtS\cdot 2H_2O$: C, 45.69; H, 3.72; N, 6.27; S, 3.59. Found: C, 45.46; H, 4.08; N, 6.44, S 3.82.

L-Pt-1. Yield 68%. The characterization data of **L-Pt-1** was in consistent with that of **D-Pt-1**.

Synthesis of Pt-2. The procedures were similar to that of complex **Pt-1**, except that **L1** was replaced by **L2** (0.1 mmol, 1.0 equiv.) to give the product as a dark-red solid.

D-Pt-2. Yield 72%. ^{1}H NMR (600 MHz, CD_3CN): δ 8.39 (s, 1H), 8.09 (d, J = 5.0 Hz, 1H), 7.84 (t, J = 7.6 Hz, 1H), 7.65 - 7.57 (m, 2H), 7.35 - 7.29 (m, 3H), 7.26 (d, J = 8.4 Hz, 3H), 7.17 (d, J = 7.9 Hz, 1H), 6.86 (d, J = 7.4 Hz, 1H), 6.74 (t, J = 7.0 Hz, 1H), 6.67 (t, J = 6.8 Hz, 1H), 6.59 (d, J = 7.1 Hz, 1H), 3.55 (d, J = 15.6 Hz, 1H), 3.14 (d, J = 15.6 Hz, 1H), 2.42 - 2.33 (m, 2H), 2.09 - 2.02 (m, 1H), 1.80 - 1.71 (m, 1H), 1.51 - 1.44 (m, 1H), 1.05 (s, 3H), 0.84 (s, 4H). ^{13}C NMR (151 MHz, CD_3CN): δ 216.43, 156.58, 154.89, 153.29, 146.54, 143.42, 141.85, 141.37, 137.14, 133.00, 129.76, 128.93, 126.66, 125.13, 120.43, 59.14, 49.84, 48.96, 43.22, 42.91, 31.91, 27.10, 26.15, 22.95, 19.64, 19.39, 13.97. HRMS (ESI) calcd for $[C_{33}H_{31}N_4O_3PtS]^+$, 758.1762; found, 758.1752. Elemental analysis calcd (%) for $C_{34}H_{31}F_3N_4O_6PtS_2\cdot 2H_2O$: C, 45.69; H, 3.72; N, 6.27; S, 3.59. Found: C, 45.42; H, 3.97; N, 6.54, S 3.62.

L-Pt-2. Yield 64%. The characterization data of **L-Pt-2** was in consistent with that of **D-Pt-2**.

Synthesis of Pt-3. To a 250 ml Schlenk flask equipped were added [Pt(C^N^N) Cl] (0.11 mmol, 1.0 equiv.), chiral alkynyl ligand **L3** (0.14 mmol, 1.3 equiv.) and CuI (0.011 mmol, 0.1

equiv.). The mixture was put under three vacuum-N_2 cycles before adding degassed CH_2Cl_2 (15 mL) and *i*-Pr_2NH (5 mL). After stirring at room temperature for 24 h in darkness, the reaction mixture was concentrated under reduced pressure. Then the crude product was purified by chromatography column (silica gel, 100-200 mesh, CH_2Cl_2) and washed with Et_2O and Hexane solution.[3] The compound was obtained as brown orange powder.

D-Pt-3. Yield 45%. ^{1}H NMR (600 MHz, $CDCl_3$): δ 9.68 (s, 1H), 9.12 (d, J = 5.0 Hz, 1H), 7.95 (t, J = 7.7 Hz, 2H), 7.85 (d, J = 7.8 Hz, 1H), 7.73 (t, J = 7.9 Hz, 1H), 7.55 (d, J = 8.2 Hz, 3H), 7.53 - 7.44 (m, 4H), 7.31 (d, J = 7.6 Hz, 1H), 7.18 (t, J = 7.4 Hz, 1H), 7.04 (t, J = 7.5 Hz, 1H), 2.68 - 2.56 (m, 2H), 2.26 - 2.18 (m, 1H), 2.13 (t, J = 5.3 Hz, 1H), 2.06 (d, J = 18.6 Hz, 1H), 1.76 - 1.69 (m, 1H), 1.52 - 1.49 (m, 1H), 1.36 (s, 3H), 1.05 (s, 3H). ^{13}C NMR (151 MHz, $CDCl_3$): δ 217.69, 168.30, 152.10, 140.64, 140.58, 132.67, 131.82, 129.22, 125.76, 124.67, 124.54, 120.87, 119.88, 119.73, 118.26, 66.63, 51.00, 44.30, 44.23, 29.16, 28.02, 21.14, 20.95. HRMS (ESI) calcd for $[C_{34}H_{29}N_3NaO_2Pt]^+$, 729.1803; found, 729.1799. Elemental analysis calcd (%) for $C_{34}H_{29}N_3O_2Pt\cdot 0.2CH_2Cl_2$: C, 56.76; H, 4.09; N, 5.81. Found: C, 56.62; H, 4.29; N, 5.65.

L-Pt-3. Yield 45%. The characterization data of **L-Pt-3** was in consistent with that of **D-Pt-3**.

Synthesis of Pt-4. The procedures were similar to that of complex **Pt-3**, except that **L3** was replaced by **L4** (0.1 mmol, 1.0 equiv.) to give the product as brown orange powder.

D-Pt-4. Yield 43%. ^{1}H NMR (600 MHz, $CDCl_3$): δ 9.20 (d, J = 5.4 Hz, 1H), 8.02 (t, J = 7.8 Hz, 1H), 7.96 (d, J = 7.2 Hz, 1H), 7.89 (d, J = 7.8 Hz, 1H), 7.80 (t, J = 7.8 Hz, 1H), 7.66 (s, 1H), 7.59 (d, J = 7.8 Hz, 1H), 7.57 - 7.50 (m, 4H), 7.36 (d, J = 7.8 Hz, 1H), 7.21 (d, J = 8.5 Hz, 2H), 7.18 (d, J = 7.4 Hz, 1H), 7.06 (t, J = 7.6 Hz, 1H), 3.40 (d, J = 15.3 Hz, 1H), 2.85 (d, J = 15.3 Hz, 1H), 2.50 - 2.43 (m, 1H), 2.24 - 1.93 (m, 5H), 1.51 - 1.45 (m, 1H), 0.96 (s, 3H), 0.88 (s, 3H). ^{13}C NMR (151 MHz, $CDCl_3$): δ 217.42, 165.87, 158.18, 154.61, 151.85, 146.82, 142.33, 138.81, 134.70, 132.89, 131.69, 127.66, 124.60, 123.91, 122.31, 118.57, 117.76, 77.37, 77.16, 76.95, 61.06, 59.95, 49.31, 48.94, 43.31, 43.06, 31.74, 29.85, 27.97, 27.28, 22.80, 20.12, 19.54, 14.25, 1.16. HRMS (ESI) calcd for $[C_{34}H_{31}N_3NaO_3PtS]^+$, 779.1629, found, 779.1605. Elemental analysis calcd (%) for $C_{34}H_{31}N_3O_3Pt\cdot 2H_2O$: C, 51.51; H, 4.45; N, 5.30; S, 4.04. Found: C, 51.56; H, 4.75; N, 5.43; S, 4.32.

L-Pt-4. Yield 38%. The characterization data of **L-Pt-4** was in consistent with that of **D-Pt-4**.

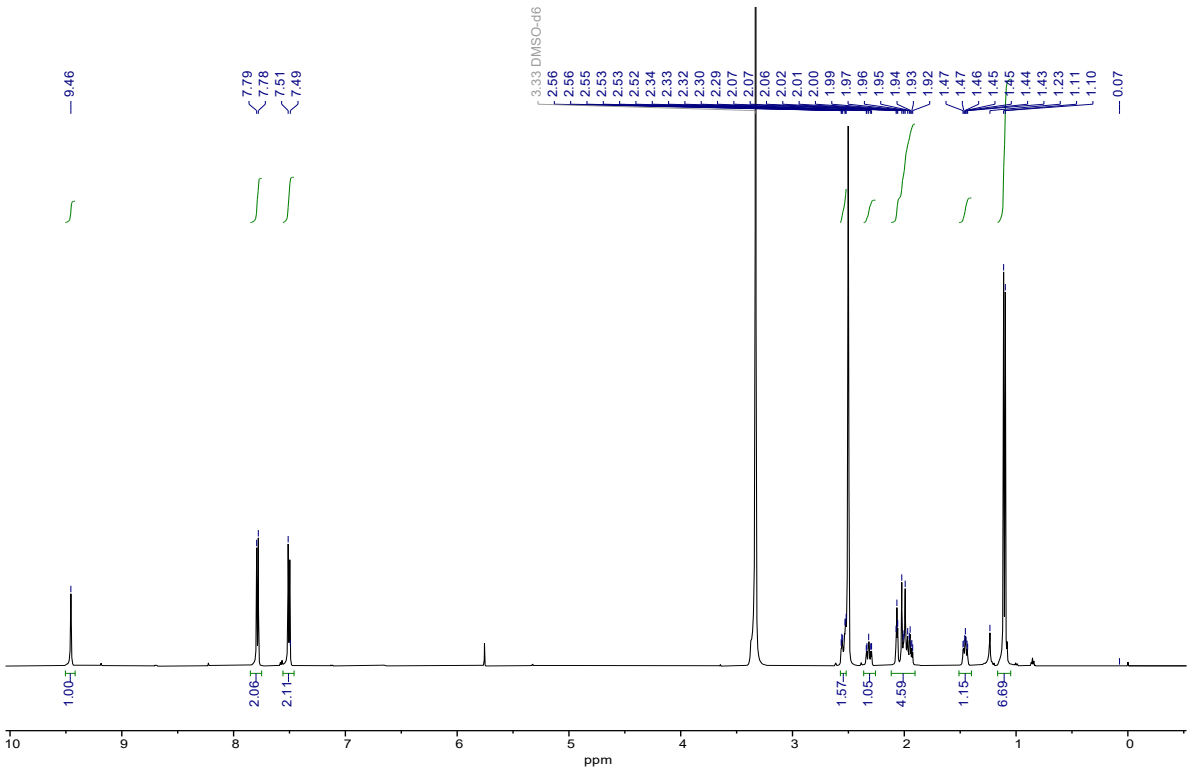

Figure S1. ^{1}H NMR spectrum of **D-L1** in DMSO.

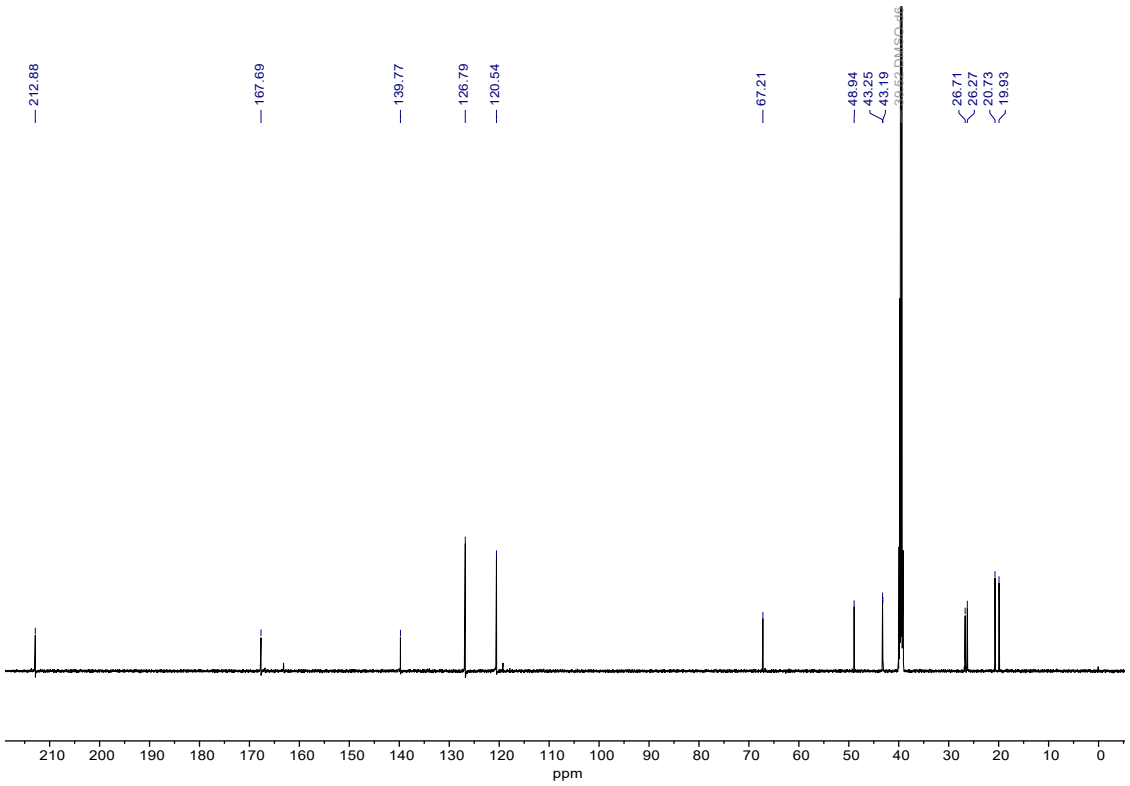

Figure S2. ^{13}C NMR spectrum of **D-L1** in $CDCl_3$.

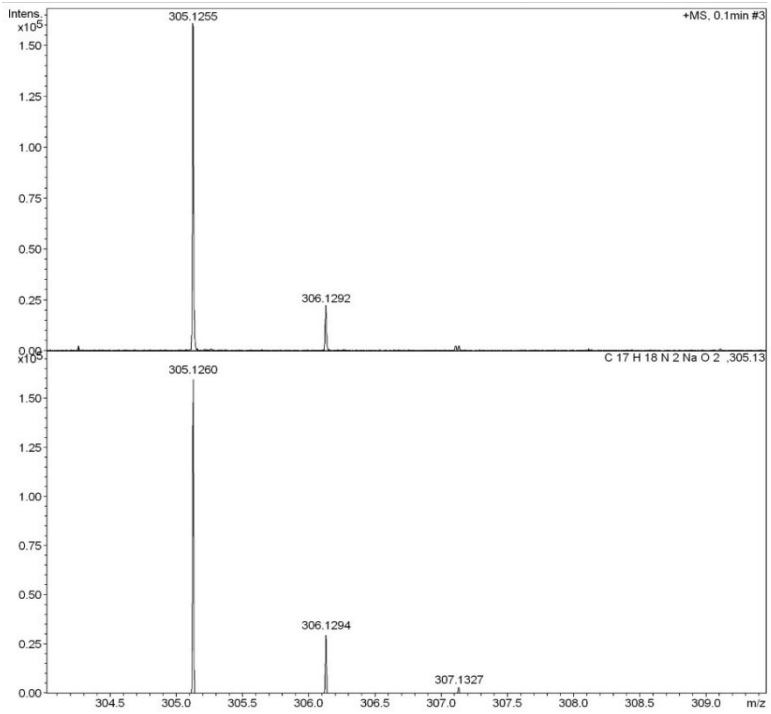

Figure S3. HRMS spectrum of **D-L1**.

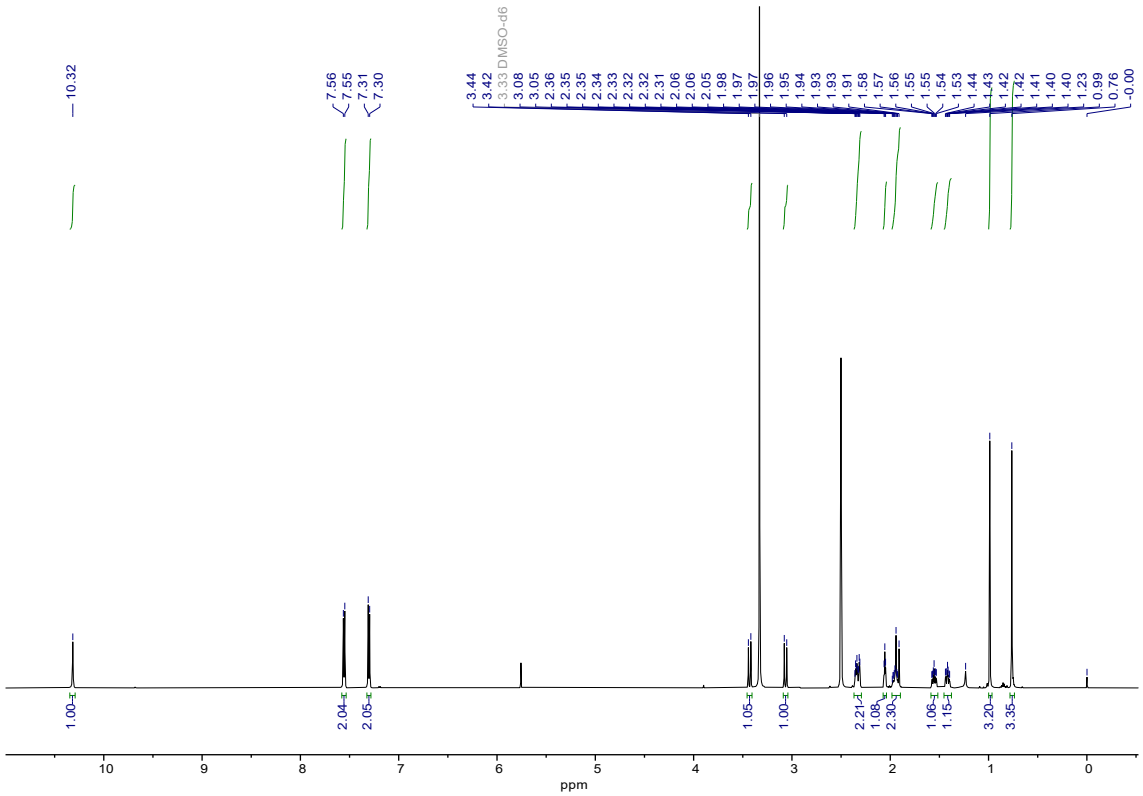

Figure S4. ^{1}H NMR spectrum of **D-L2** in DMSO.

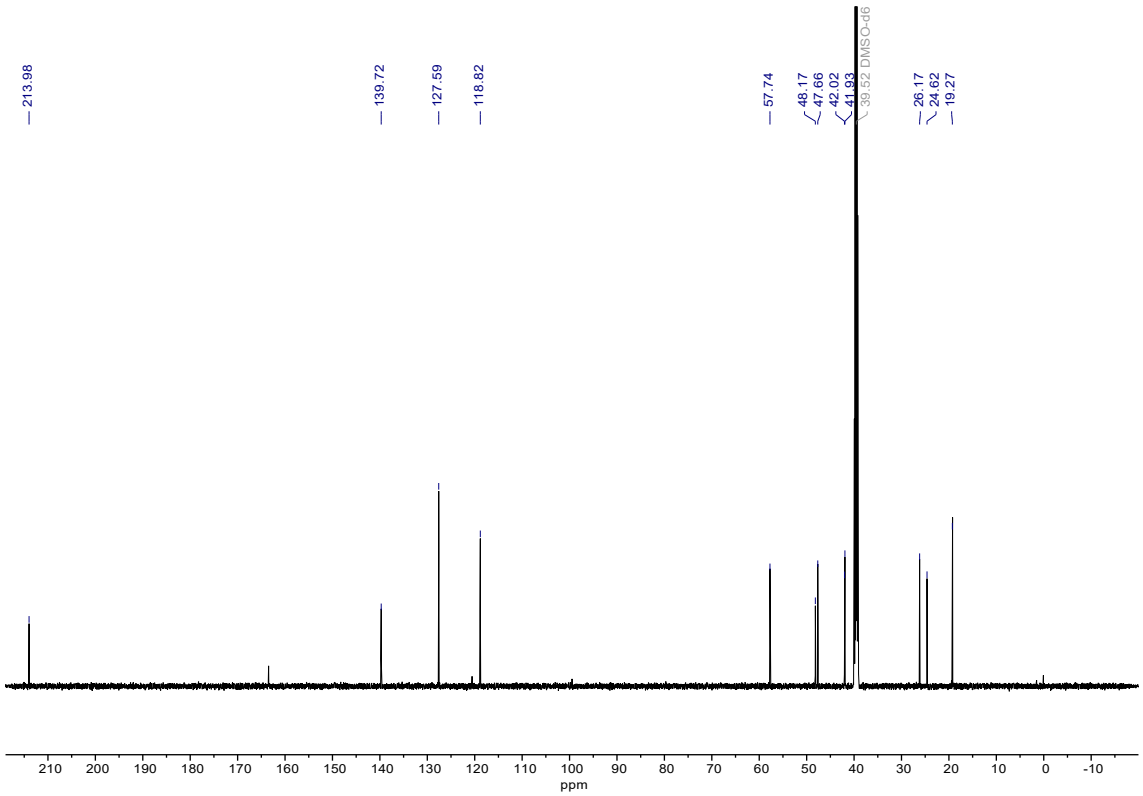

Figure S5. ^{13}C NMR spectrum of **D-L2** in DMSO.

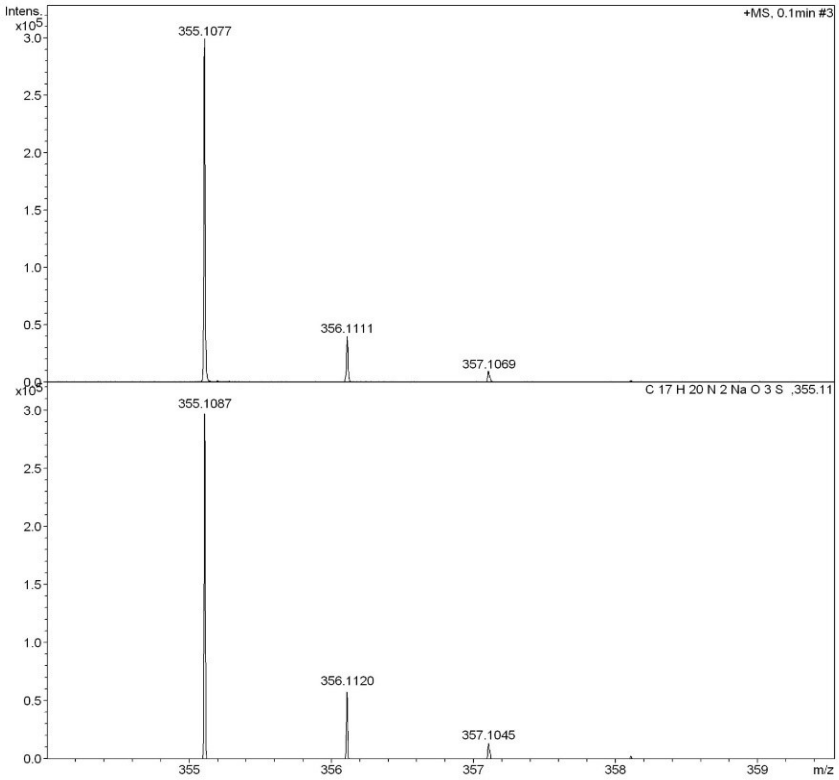

Figure S6. HMRS spectrum of **D-L2**.

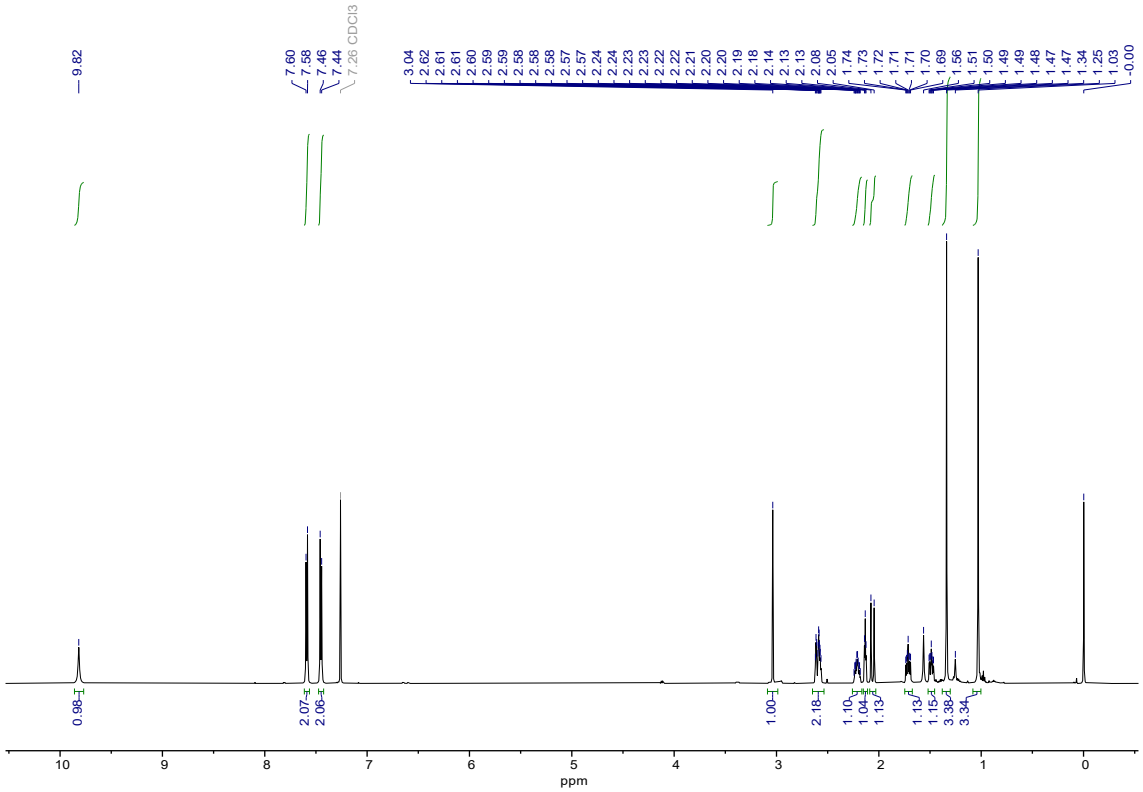

Figure S7. ^{1}H NMR spectrum of **D-L3** in $CDCl_3$.

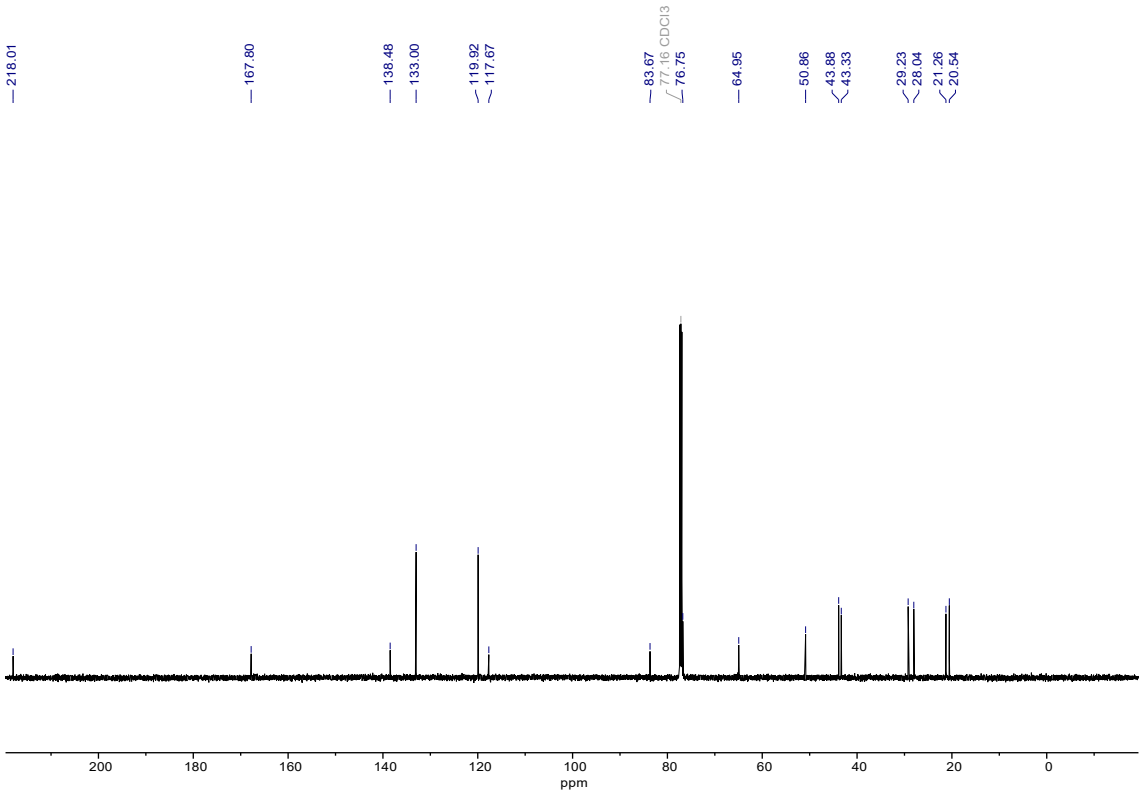

Figure S8. ^{13}C NMR spectrum of **D-L3** in $CDCl_3$.

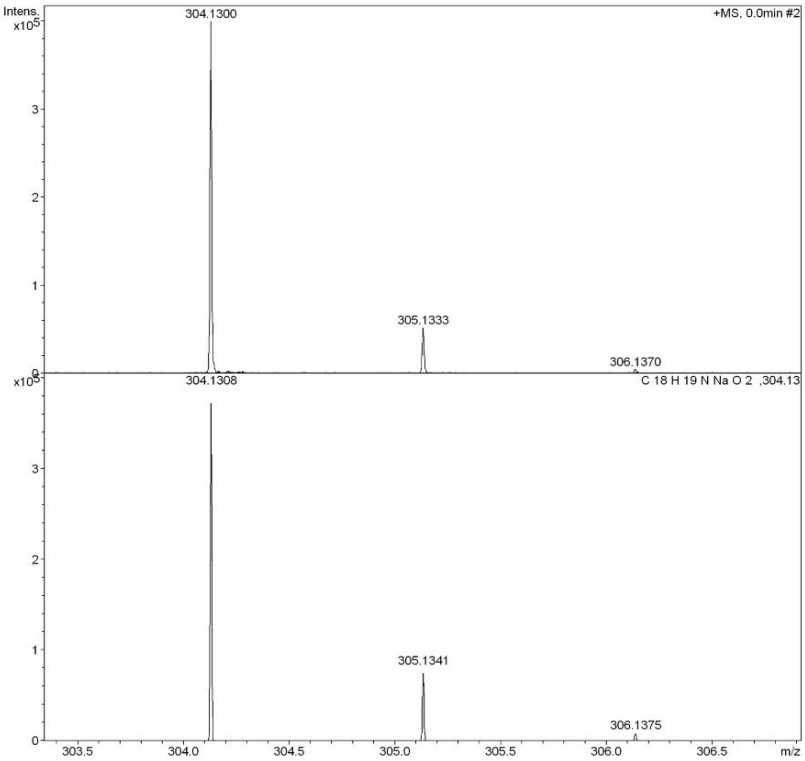

Figure S9. HRMS spectrum of **D-L3**.

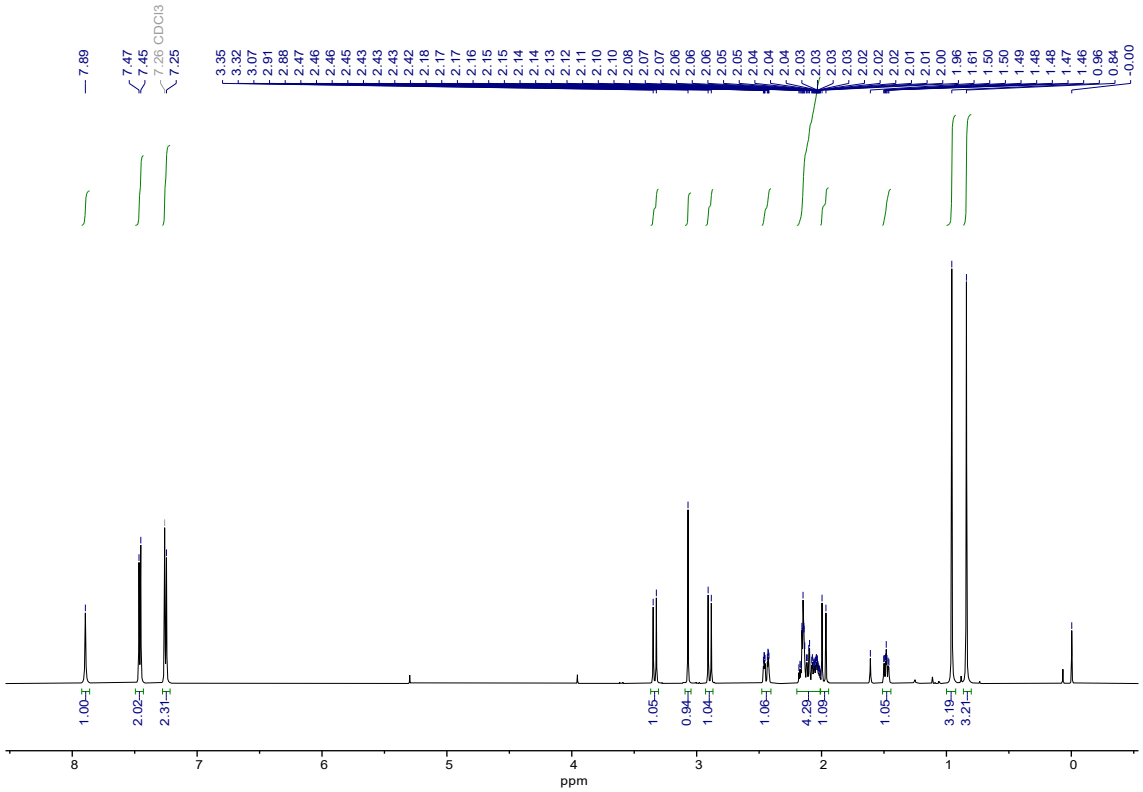

Figure S10. ^{1}H NMR spectrum of **D-L4** in $CDCl_3$.

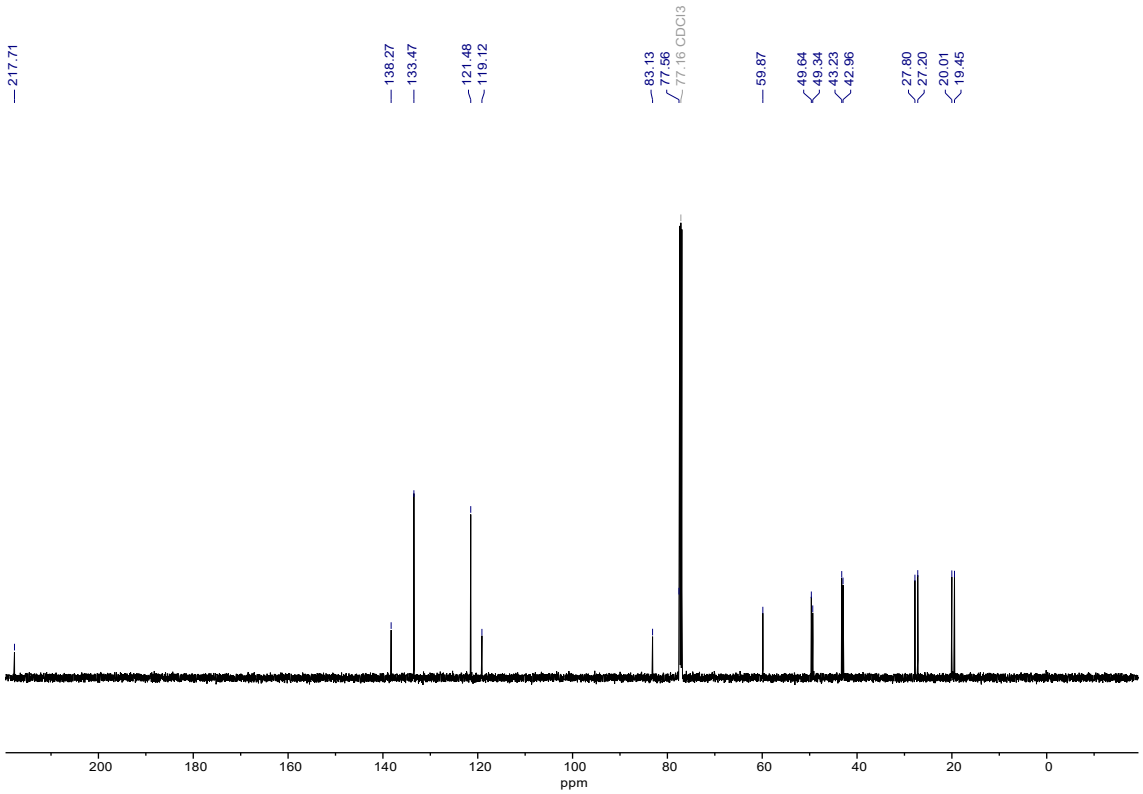

Figure S11. ^{13}C NMR spectrum of **D-L4** in $CDCl_3$.

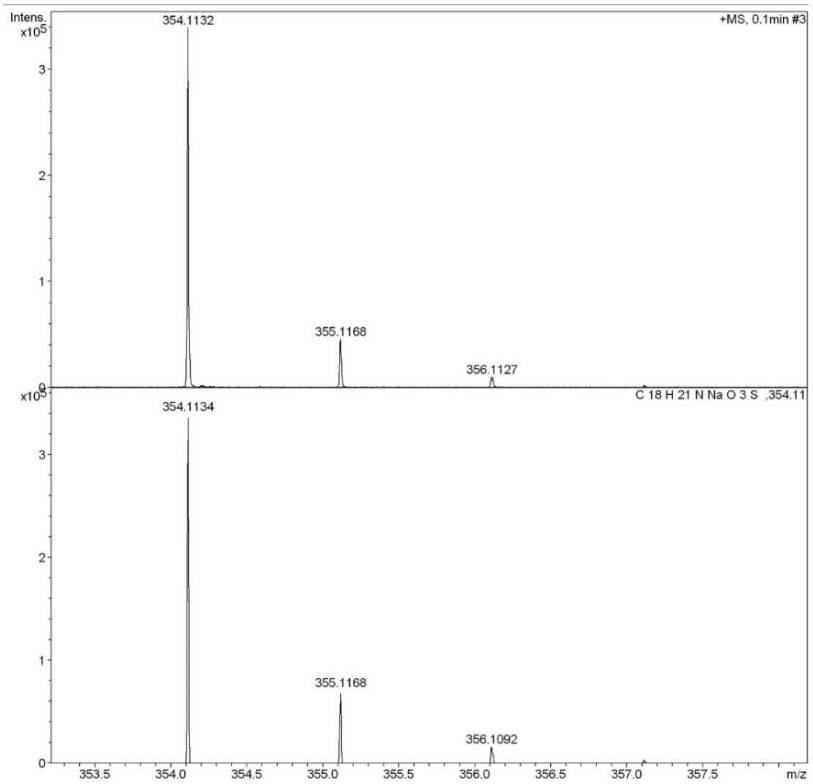

Figure S12. HRMS spectrum of **D-L4**.

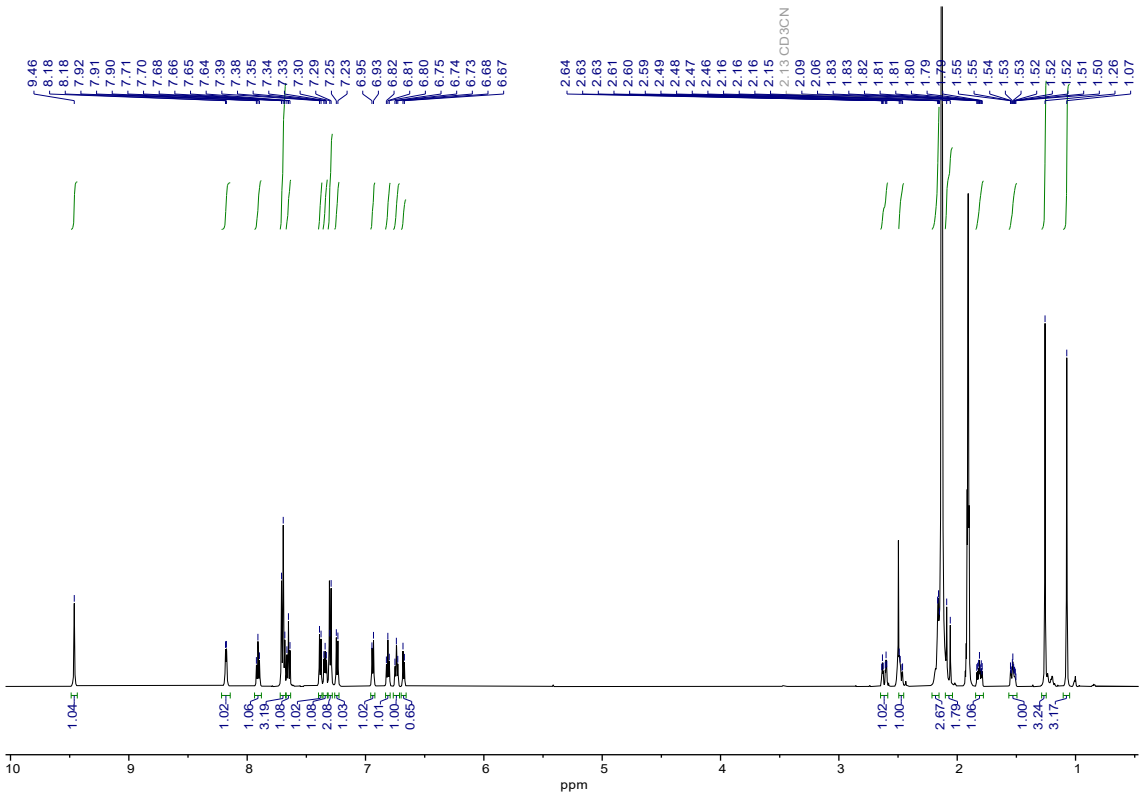

Figure S13. ^{1}H NMR spectrum of **D-Pt-1** in CD_3CN.

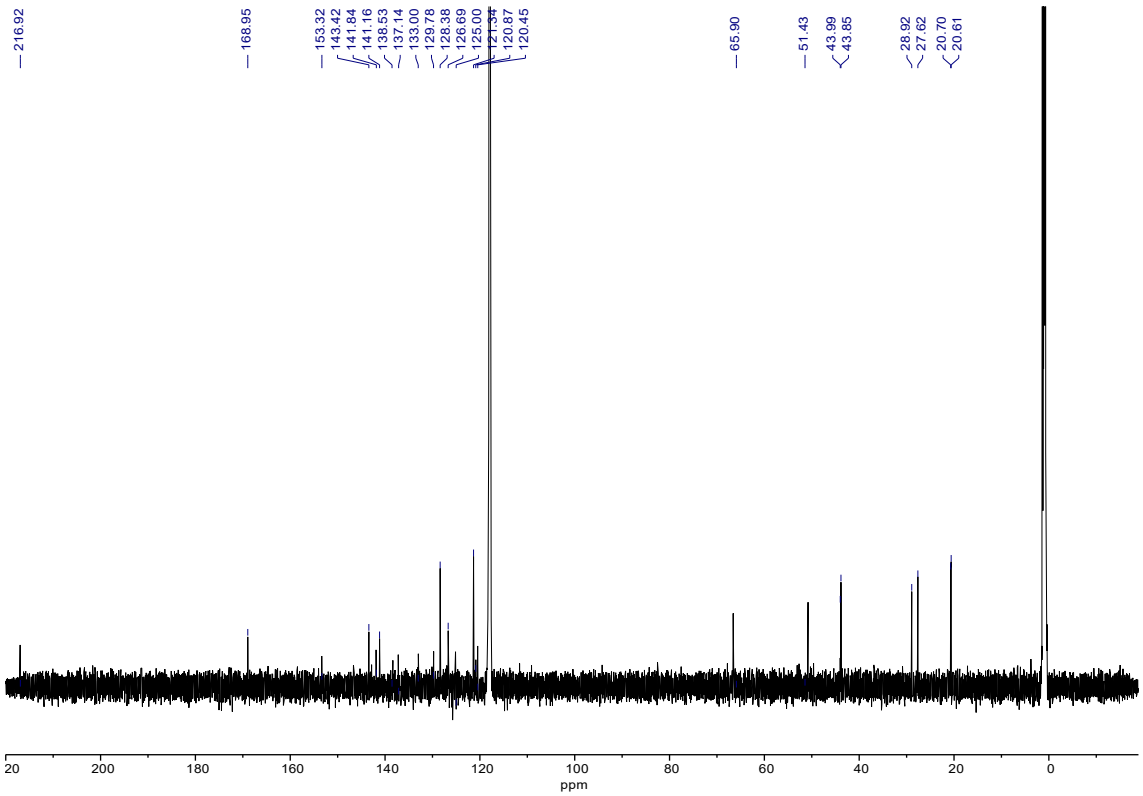

Figure S14. ^{13}C NMR spectrum of **D-Pt-1** in CD_3CN.

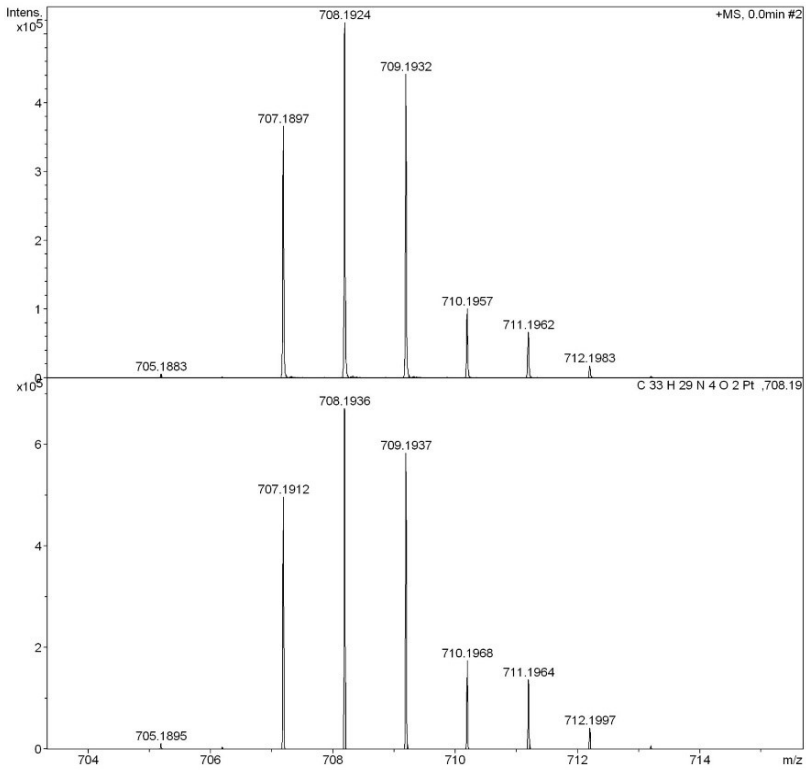

Figure S15. HRMS spectrum of **D-Pt-1** in CD_3CN.

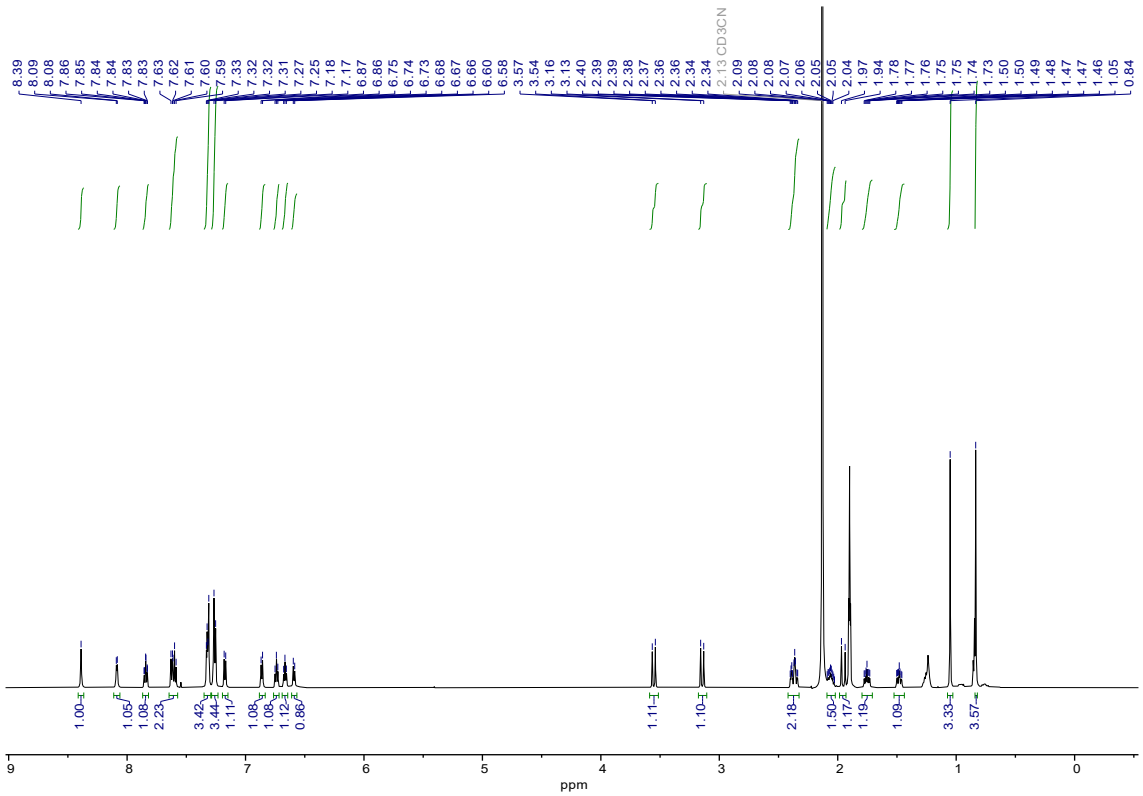

Figure S16. ^{1}H NMR spectrum of **D-Pt-2** in CD_3CN.

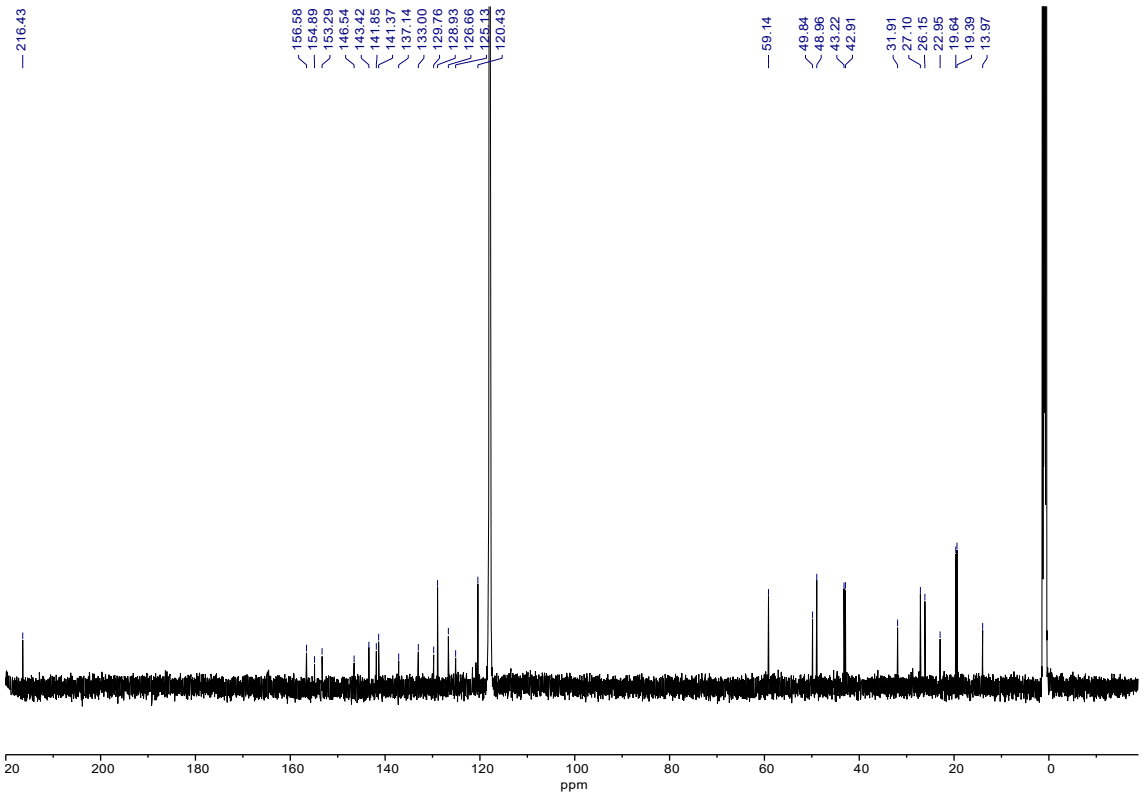

Figure S17. ^{13}C NMR spectrum of **D-Pt-2** in CD_3CN.

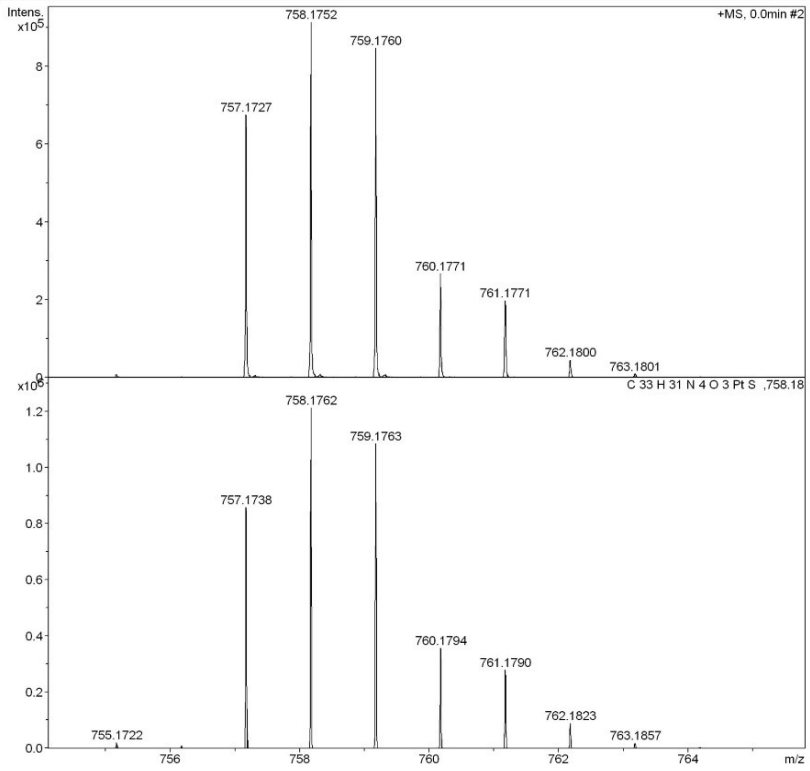

Figure S18. HRMS spectrum of **D-Pt-2**.

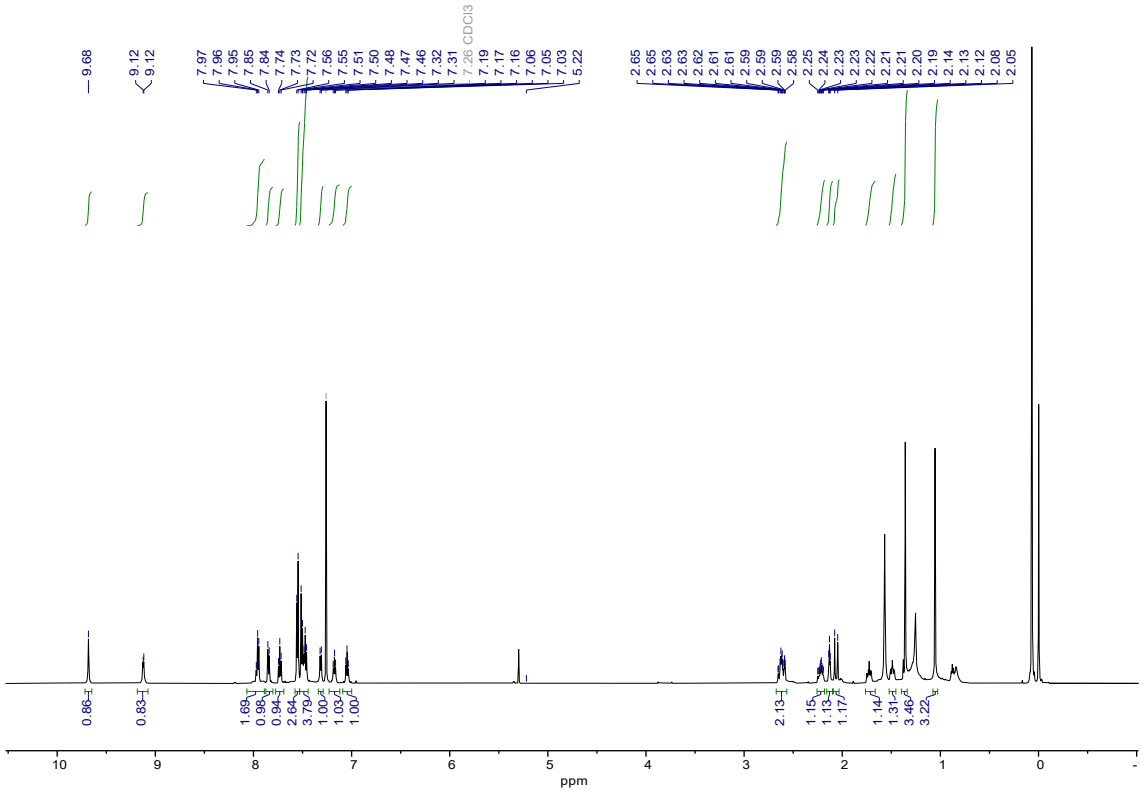

Figure S19. ^{1}H NMR spectrum of **D-Pt-3** in $CDCl_3$.

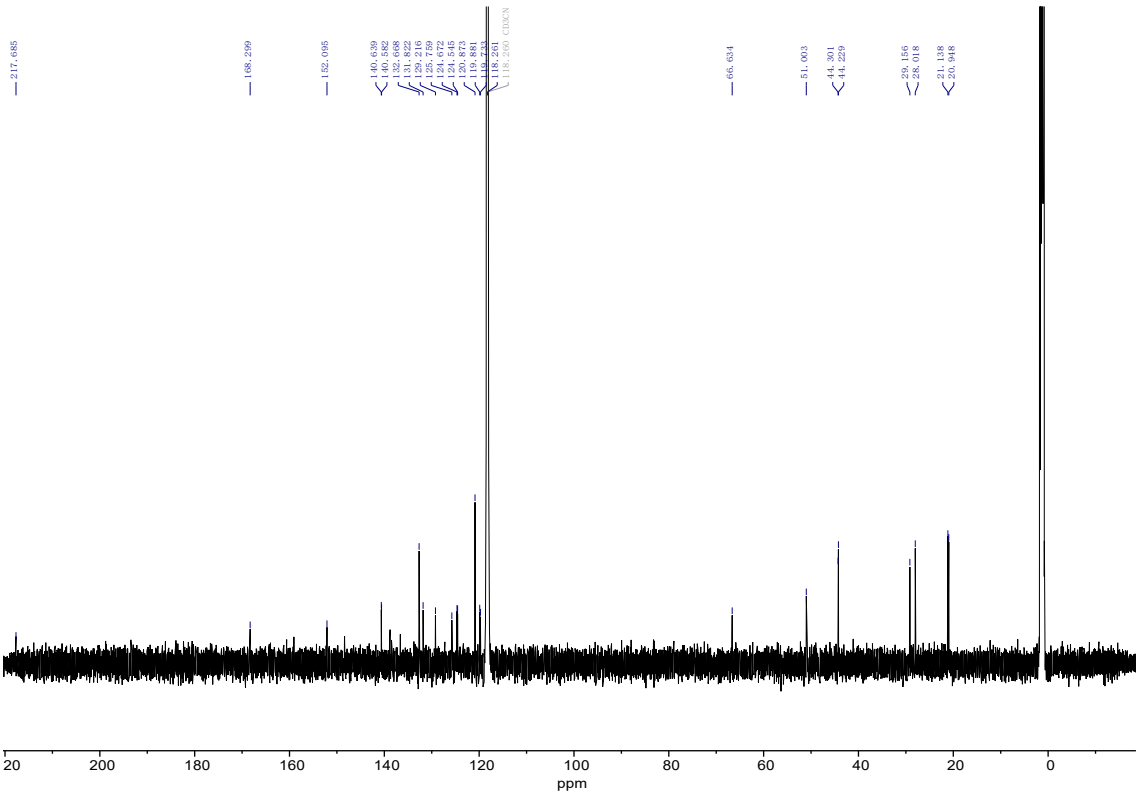

Figure S20. ^{13}C NMR spectrum of **D-Pt-3** in $CDCl_3$.

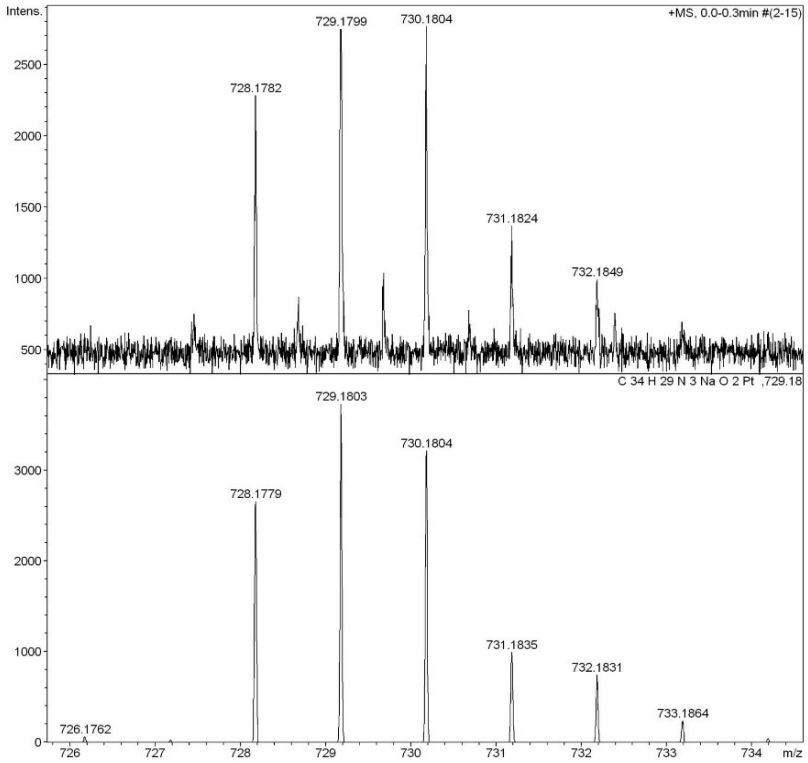

Figure S21. HRMS spectrum of **D-Pt-3**.

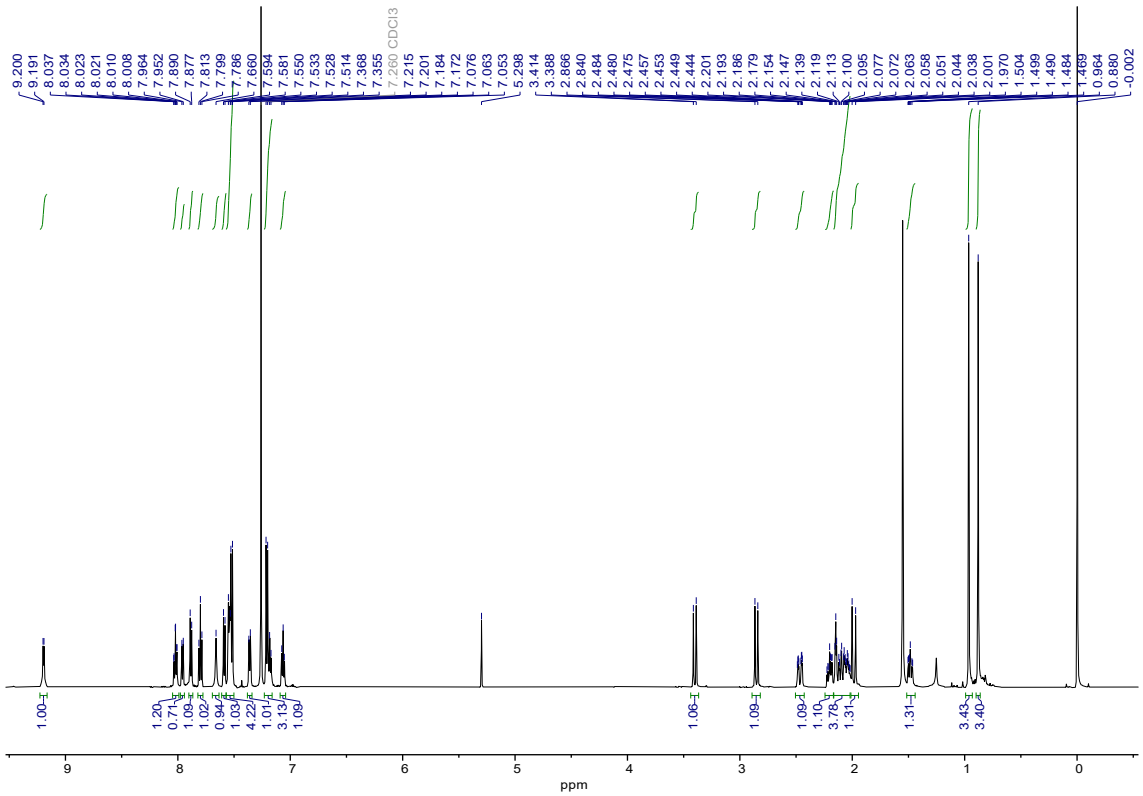

Figure S22. ^{1}H NMR spectrum of **D-Pt-4** in $CDCl_3$.

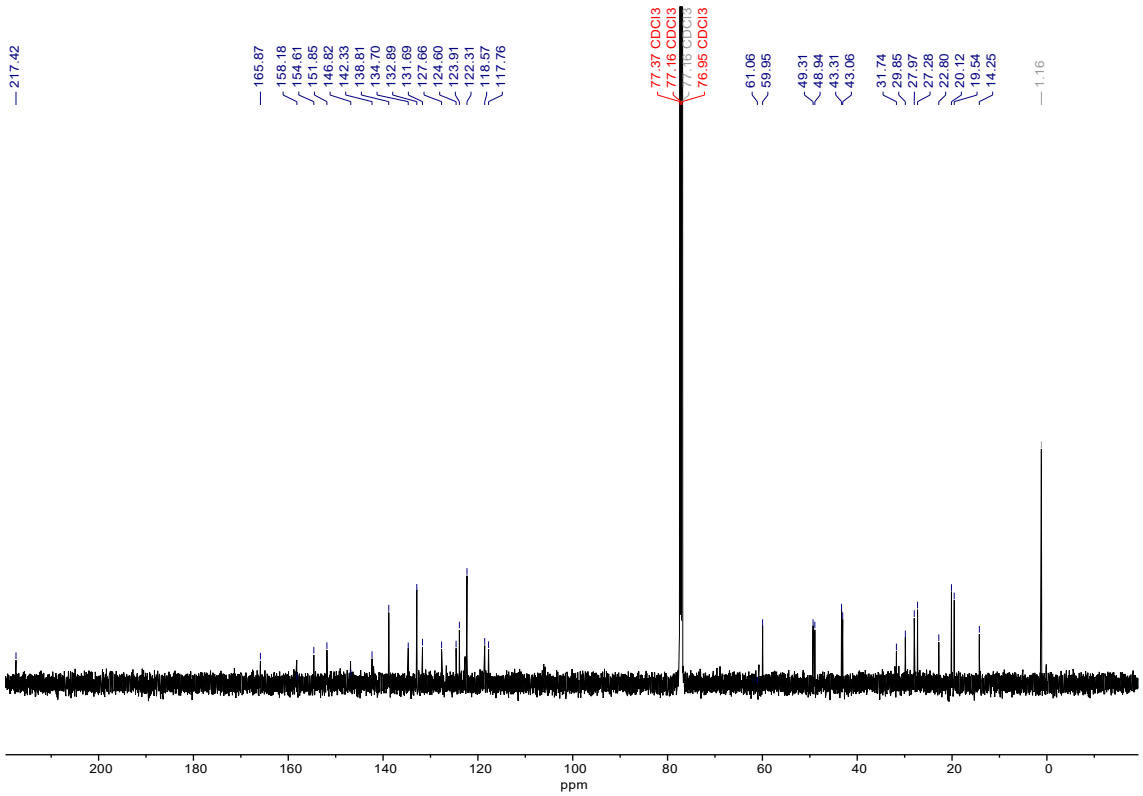

Figure S23. ^{13}C NMR spectrum of **D-Pt-4** in $CDCl_3$.

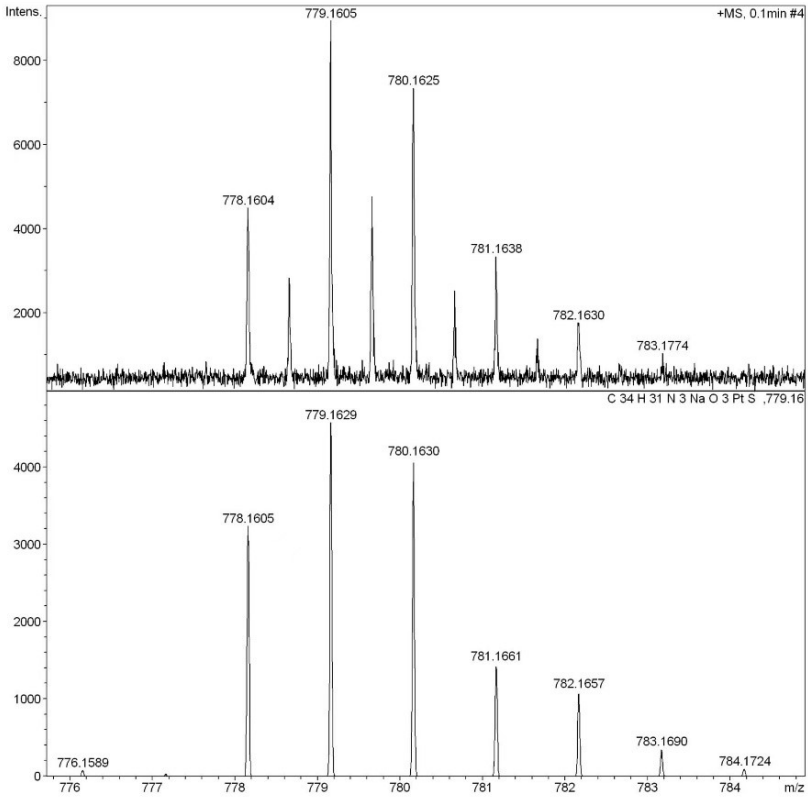

Figure S24. HRMS spectrum of **D-Pt-4**.

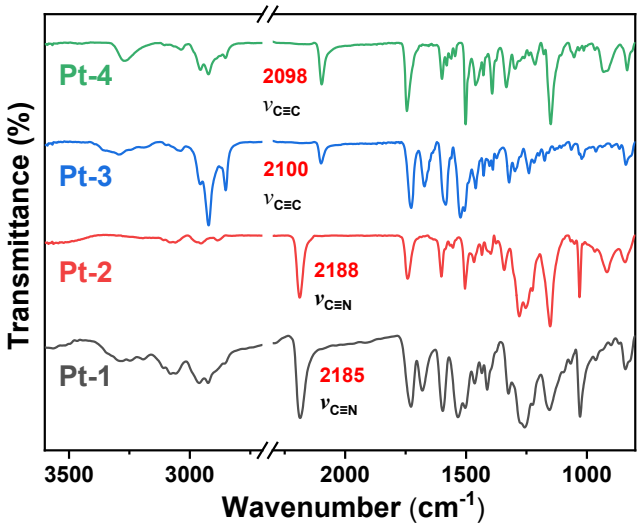

Figure S25. FT-IR spectra of complexes **Pt-1~Pt-4**.

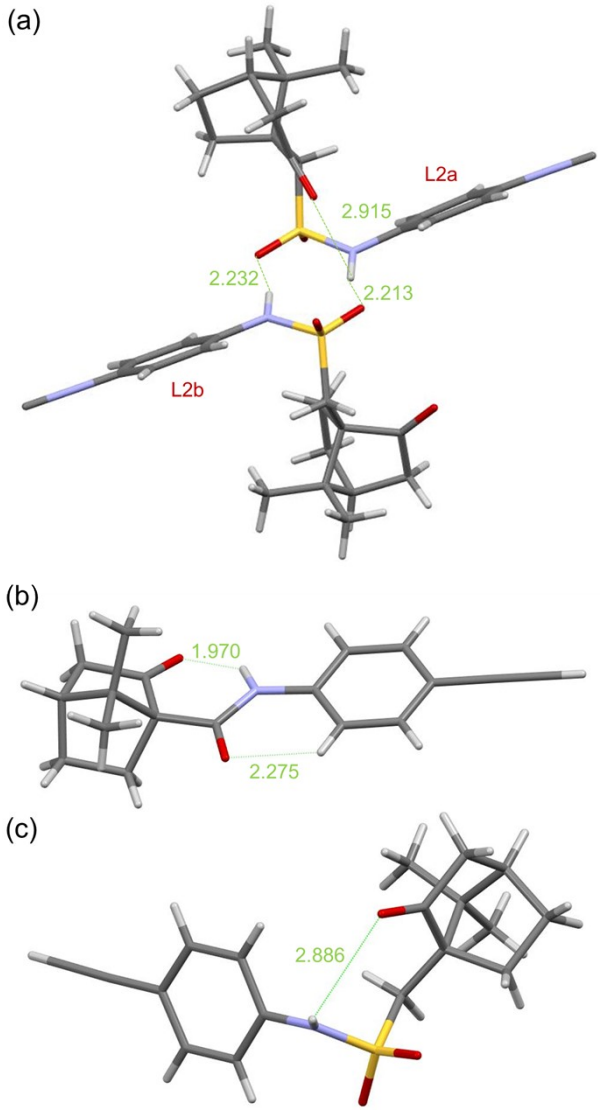

Figure S26. Single crystal structures of (a) **L2** (CCDC 2209736), (b) **L3** (CCDC 2209733) and (c) **L4** (CCDC 2209735). Green dotted lines, intramolecular N-H···O=C interactions.

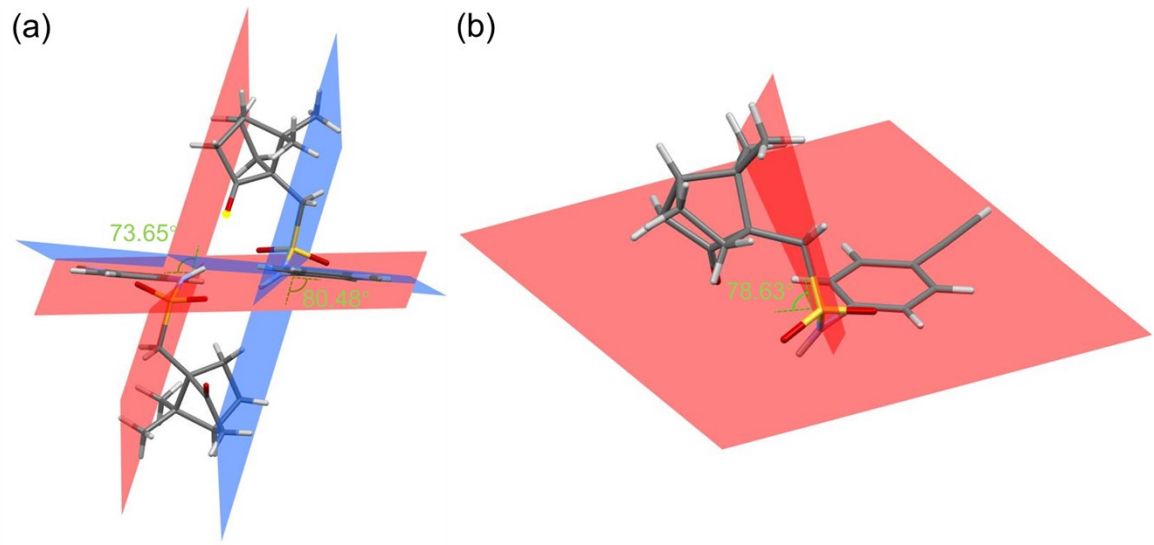

Figure S27. Dihedral angles in the X-ray crystal structure of ligands (a) **L2** and (b) **L4**.

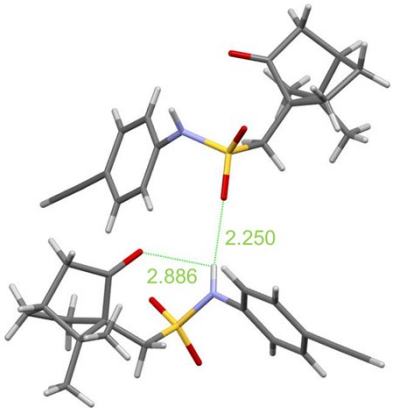

Figure S28. Molecular packing of ligand **L4**.

Table S1. Crystallographic data of single crystal for **L2-L4**.

	***D*-L2 (CCDC 2209736)**	***L*-L3 (CCDC 2209733)**	***L*-L4 (CCDC 2209735)**
Empirical formula	$C_{17}H_{20}N_2O_3S$	$C_{18}H_{19}NO_2$	$C_{18}H_{21}NO_3S$
Formula weight	332.41	281.34	331.42
Temperature/K	250.00	153.00	153.15
Crystal system	triclinic	orthorhombic	orthorhombic
Space group	P1	$P2_12_12_1$	$P2_12_12_1$
a/Å	7.1344(6)	11.2317(5)	8.7823(6)
b/Å	10.1798(9)	11.5042(5)	10.1497(6)
c/Å	11.5186(10)	11.6690(5)	18.5221(12)
α/°	105.967(2)	90	90
β/°	92.665(2)	90	90
γ/°	91.935(2)	90	90
Volume/Å^3	802.47(12)	1507.77(11)	1651.02(18)
Z	2	4	4
ρ_{calc}g/cm^3	1.376	1.239	1.333
μ/mm^{-1}	1.936	0.640	1.862
F(000)	352.0	600.0	704.0
Crystal size/mm^3	0.4 × 0.3 × 0.1	0.5 × 0.4 × 0.3	0.5 × 0.4 × 0.3
Radiation	CuKα (λ = 1.54178)	CuKα (λ = 1.54178)	CuKα (λ = 1.54178)
2Θ range for data collection/°	14.402 to 136.684	15.78 to 136.344	13.332 to 136.518
Index ranges	$-8 \le h \le 8$, $-12 \le k \le 12$, $-13 \le l \le 13$	$-13 \le h \le 13$, $-13 \le k \le 13$, $-14 \le l \le 14$	$-10 \le h \le 10$, $-12 \le k \le 12$, $-22 \le l \le 22$
Reflections collected	21268	20678	23753
Independent reflections	5496 [R_{int} = 0.0316, R_{sigma} = 0.0281]	2699 [R_{int} = 0.0245, R_{sigma} = 0.0130]	2975 [R_{int} = 0.0471, R_{sigma} = 0.0265]
Data/restraints/parameters	5496/3/419	2699/0/196	2975/0/211
Goodness-of-fit on F^2	1.028	1.075	1.104
Final R indexes [I>=2σ (I)]	R_1 = 0.0289, wR_2 = 0.0788	R_1 = 0.0262, wR_2 = 0.0667	R_1 = 0.0306, wR_2 = 0.0822
Final R indexes [all data]	R_1 = 0.0290, wR_2 = 0.0790	R_1 = 0.0262, wR_2 = 0.0668	R_1 = 0.0307, wR_2 = 0.0823
Largest diff. peak/hole / e Å^{-3}	0.36/-0.43	0.16/-0.13	0.39/-0.35
Flack parameter	0.088(6)	0.07(3)	0.10(2)

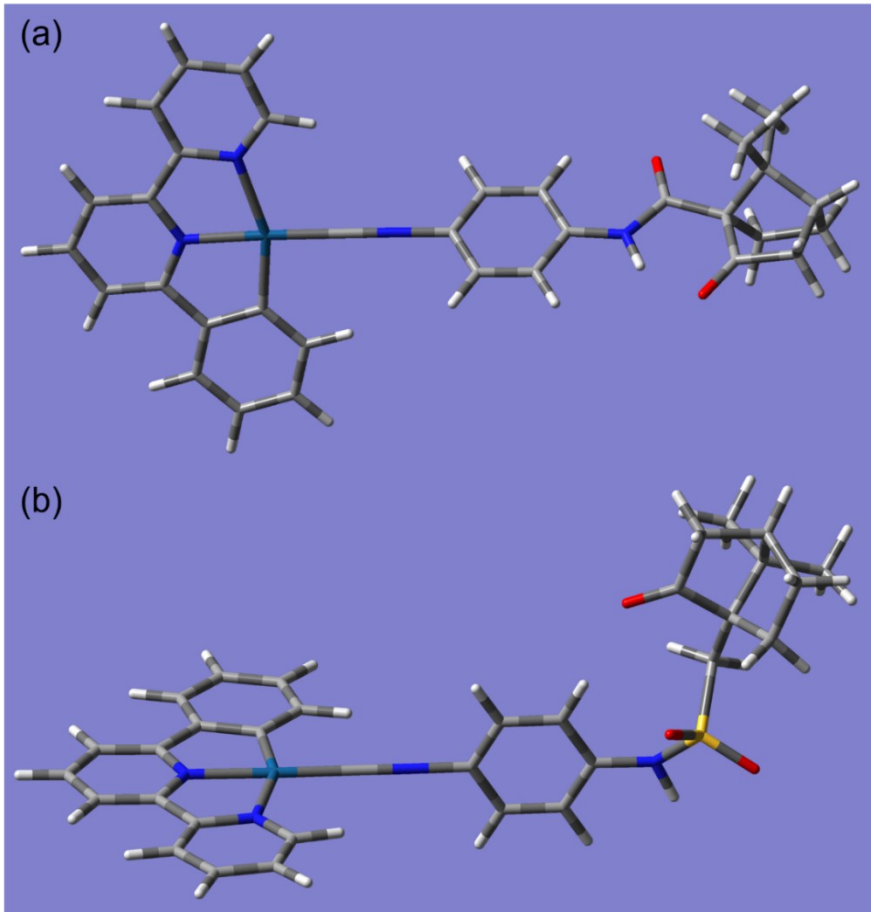

Figure S29. Optimized ground-state geometries of **Pt-1** (a) and **Pt-2** (b) in CH_3CN at the DFT level of theory.

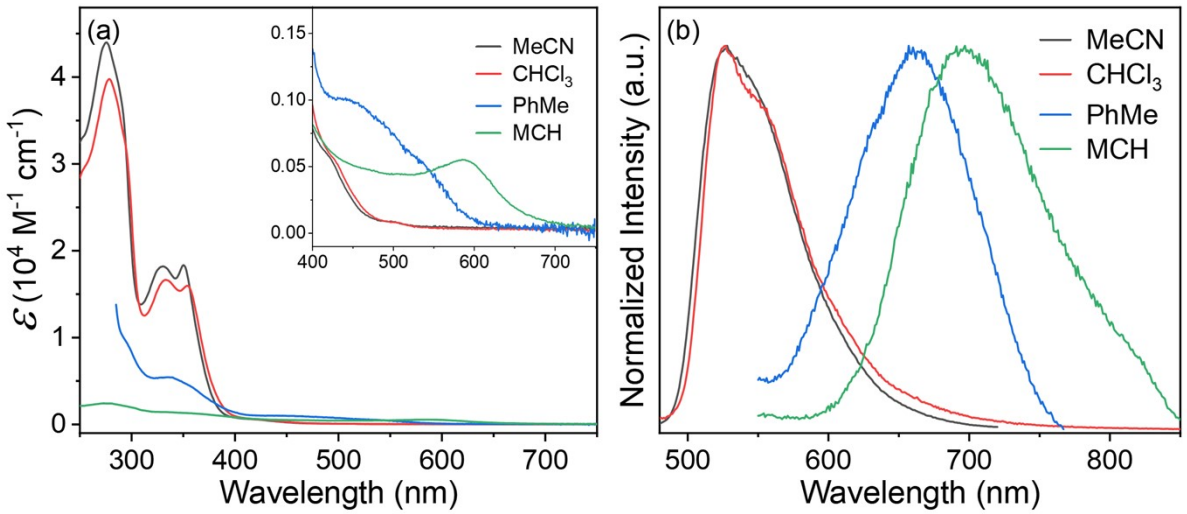

Figure S30. (a) UV-vis and (b) Emission spectra (excited at 420 nm in MeCN and $CHCl_3$, and 450 nm in toluene and MCH) of **Pt-1** in different solvents. Inset: the expanded UV-Vis absorption spectra of **Pt-1** beyond 400 nm.

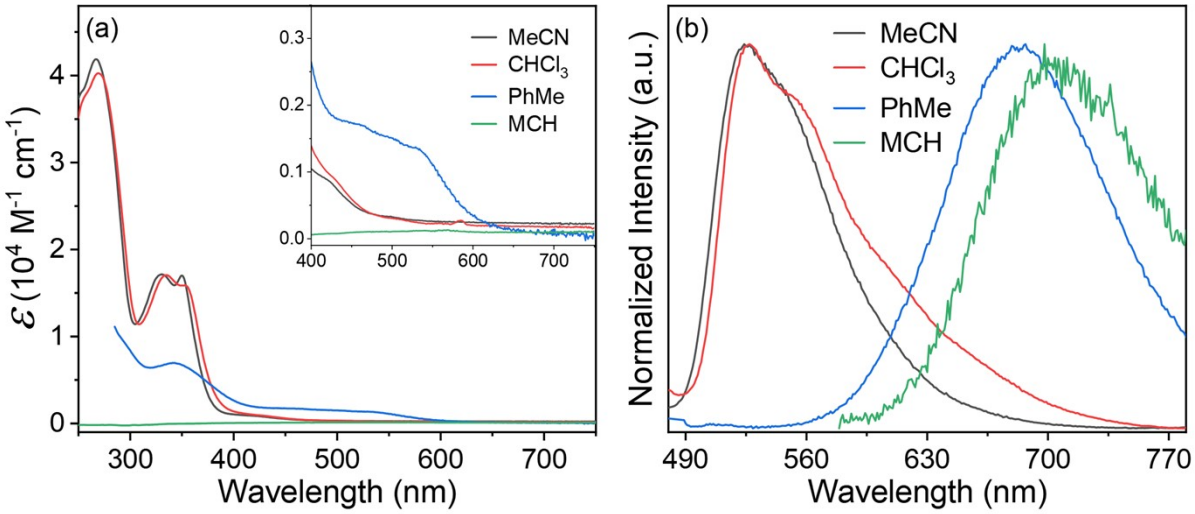

Figure S31. (a) UV-vis and (b) Emission spectra excited at 420 nm of **Pt-2** in different solvents. Inset: the expanded UV-Vis absorption spectra of **Pt-2** beyond 400 nm.

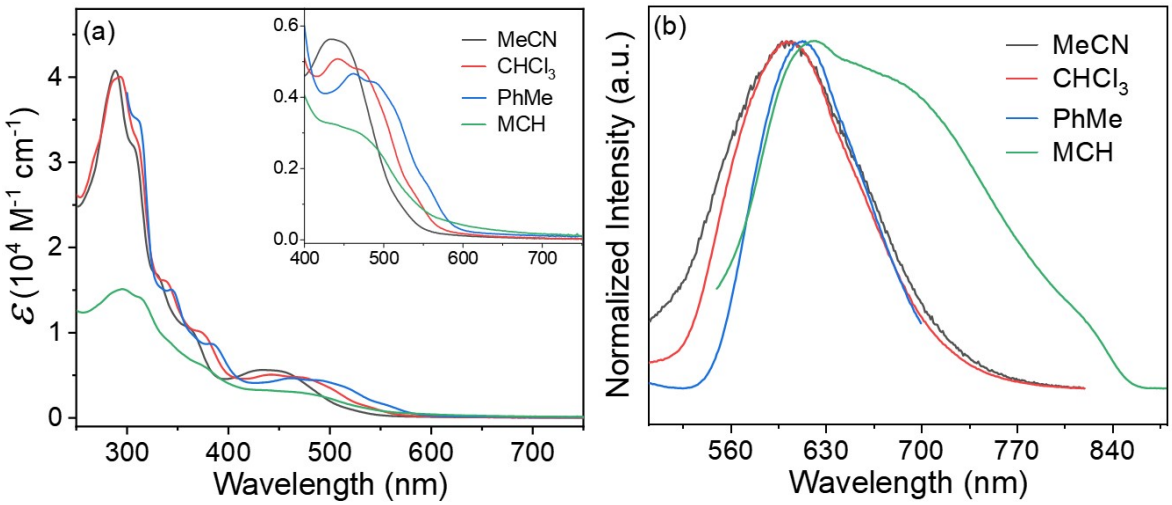

Figure S32. (a) UV-vis and (b) Emission spectra excited at 420 nm of **Pt-3** in different solvents. Inset: the expanded UV-Vis absorption spectra of **Pt-3** beyond 400 nm.

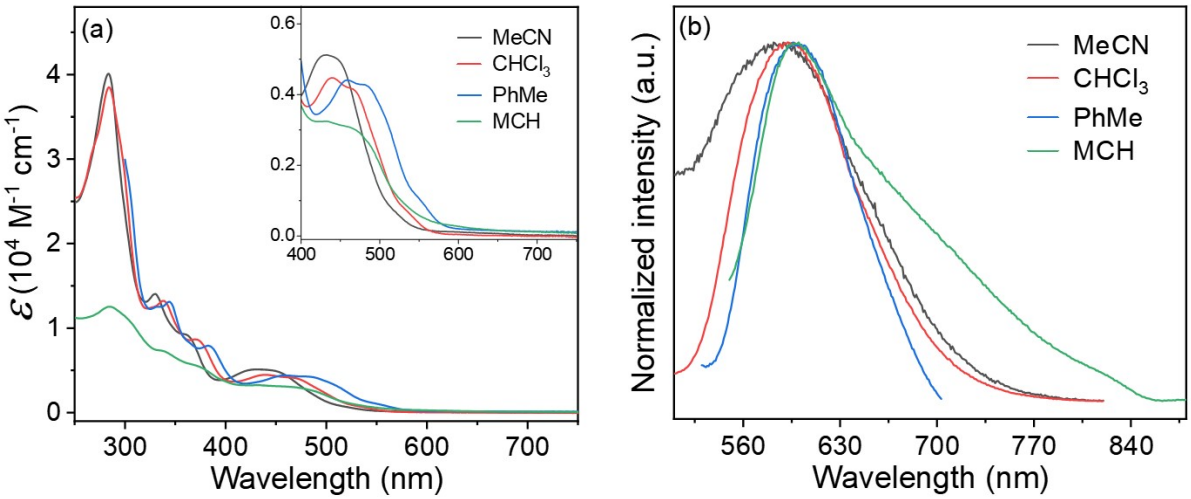

Figure S33. (a) UV-vis and (b) Emission spectra excited at 420 nm of **Pt-4** in different solvents. Inset: the expanded UV-Vis absorption spectra of **Pt-4** beyond 400 nm.

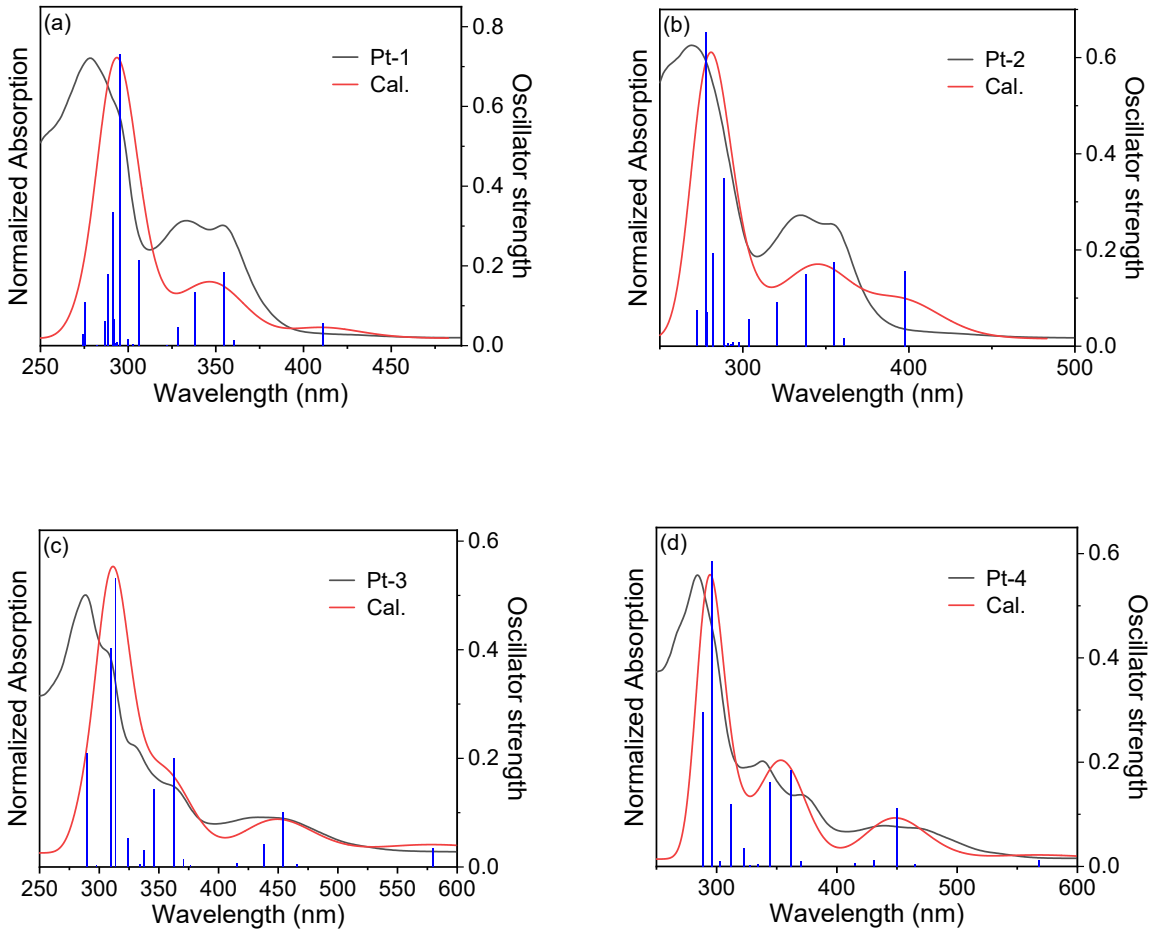

Figure S34. Comparison of the experimental and theoretical absorption spectra for **Pt-1**~**Pt-4** in chloroform.

Table S2. Natural Transition Orbitals (NTOs) Representing the Lowest Energy Transitions

	Excited states and properties	Hole	Electron
Pt-1	S1 442 nm f = 0.0009	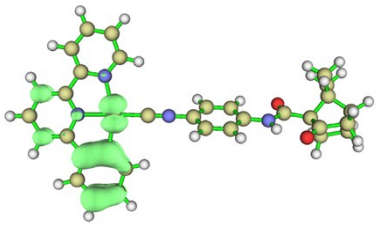	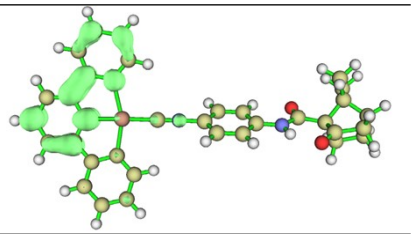
	S2 411 nm f = 0.0561	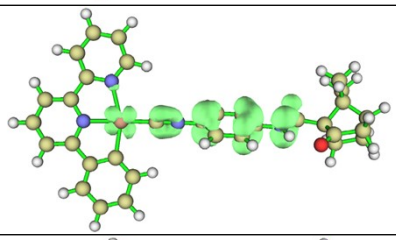	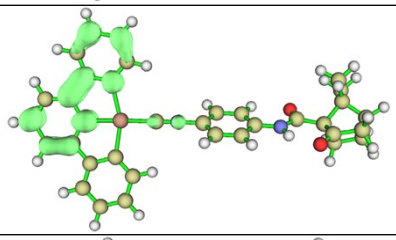
Pt-2	S1 443 nm f = 0.0009	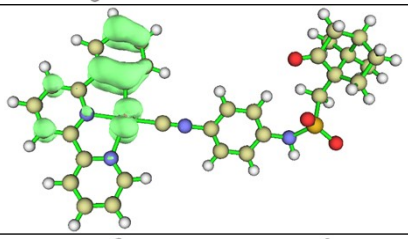	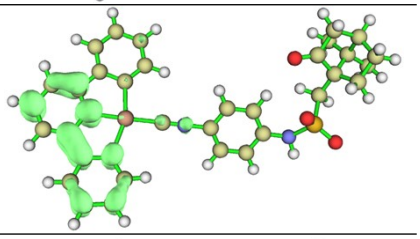
	S2 397 nm f = 0.156	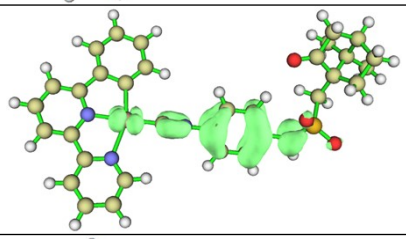	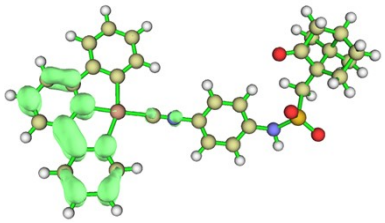
Pt-3	S1 580 nm f = 0.035	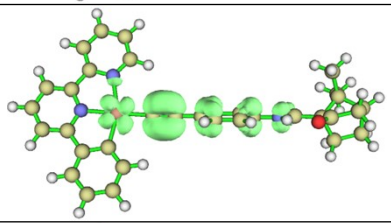	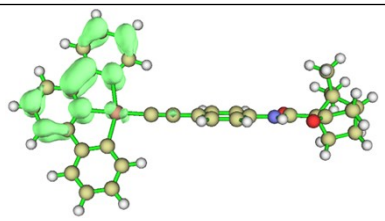
	S2 466 nm f = 0.0045	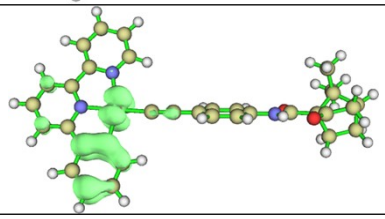	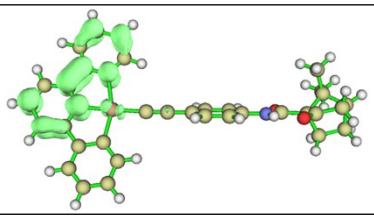

Pt-4	S1 567 nm f = 0.0126	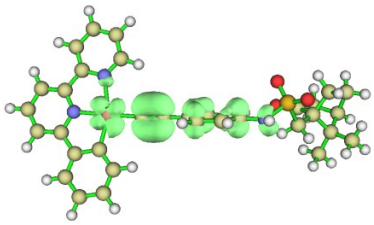	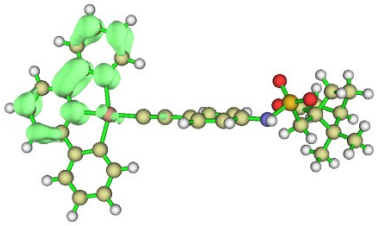
	S2 465 nm f = 0.0039	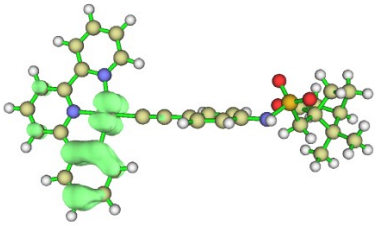	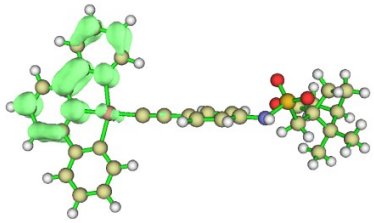

Table S3. Natural transition orbitals (NTOs) representing the major transitions contributing to the absorption bands between 280 nm-400 nm.

	Excited states and properties	Hole	Electron
Pt-1	S4 354 nm f = 0.184	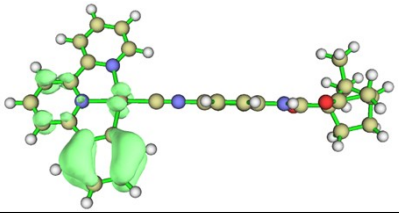	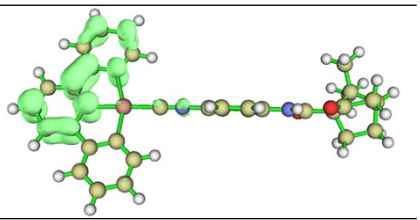
	S5 338 nm f = 0.134	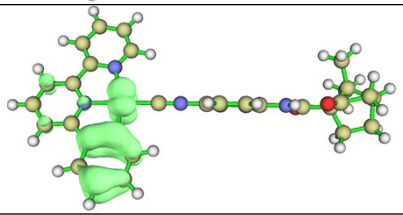	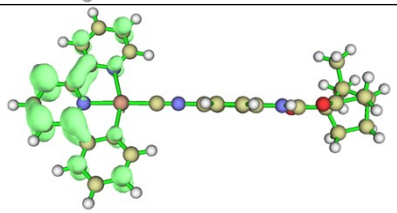
	S8 306 nm f = 0.215	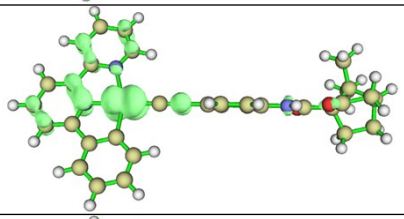	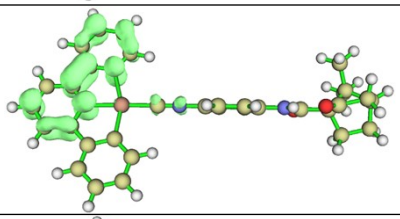
	S11 295 nm f = 0.731	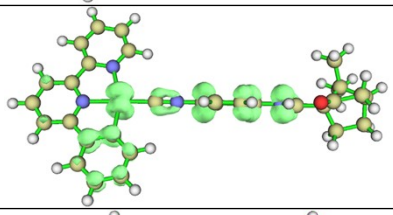	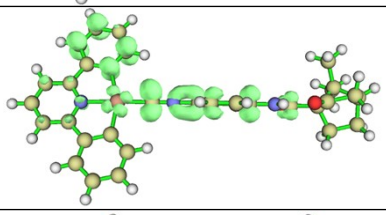
Pt-2	S4 354 nm f = 0.174	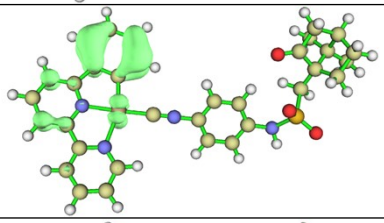	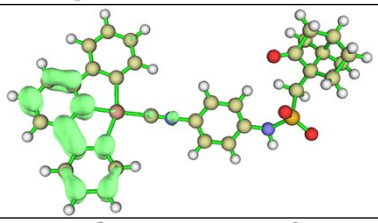
	S6 338 nm f = 0.150	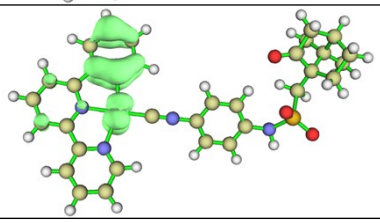	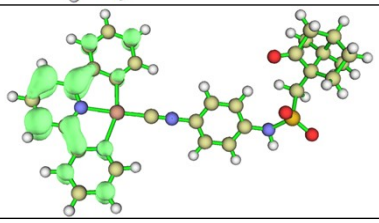

	S7 320 nm f = 0.0914	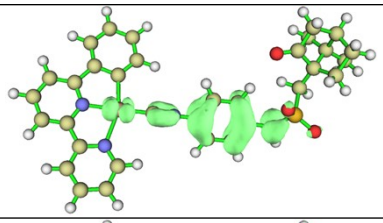	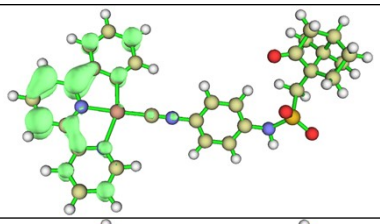
	S11 303 nm f = 0.057	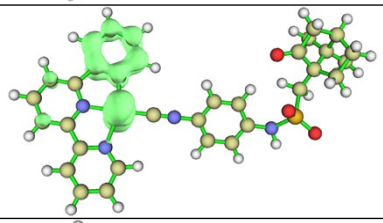	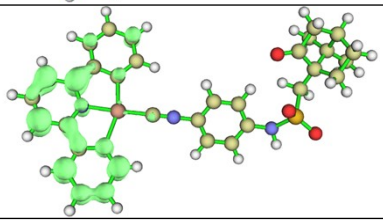
Pt-3	S3 454 nm f = 0.1006	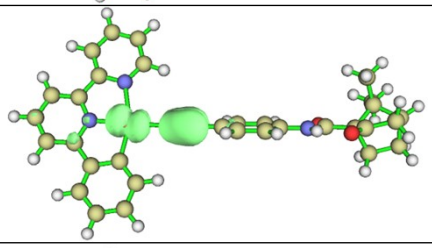	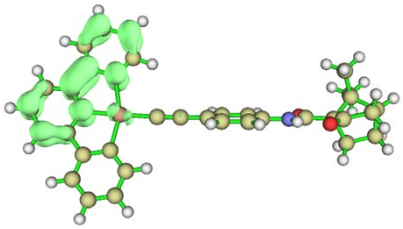
	S4 438 nm f = 0.0405	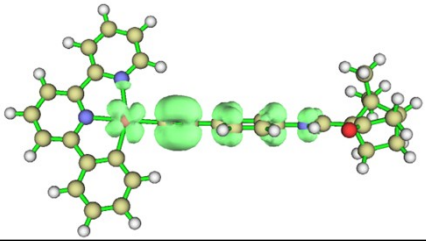	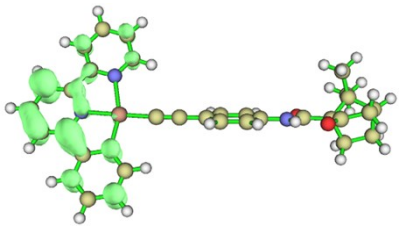
	S8 362 nm f = 0.1991	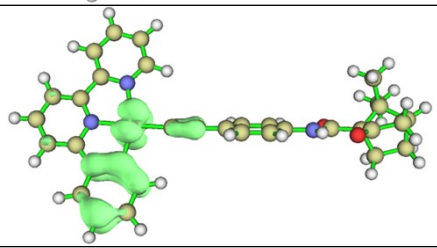	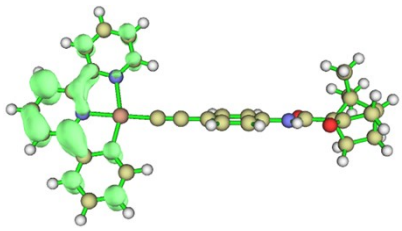
	S9 345 nm f = 0.1433	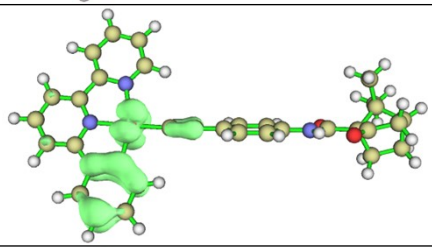	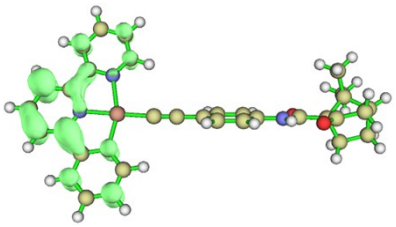
	S14 314 nm f = 0.5321	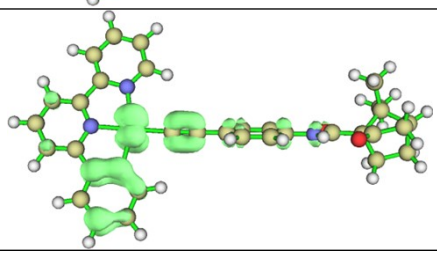	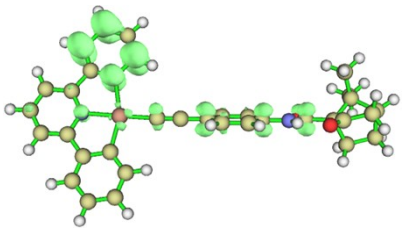

	S15 310 nm f = 0.4016	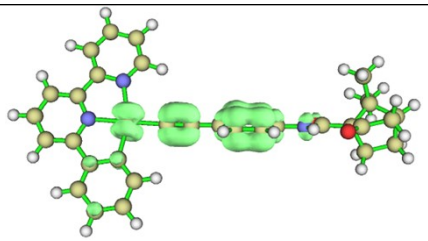	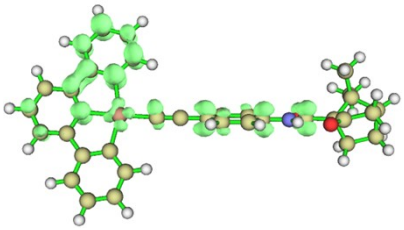
	S16 309 nm f = 0.1907	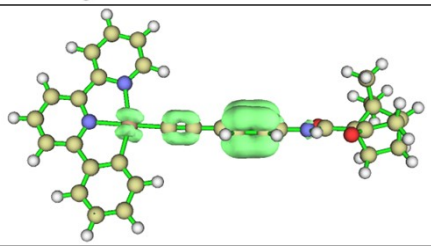	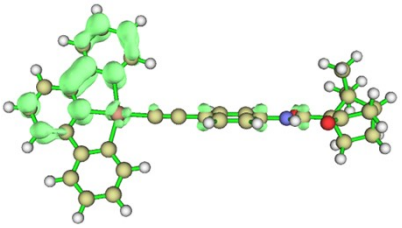
Pt-4	S3 450 nm f = 0.1125	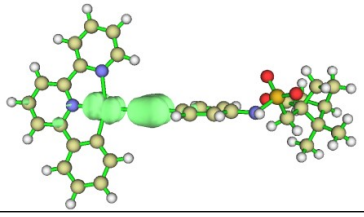	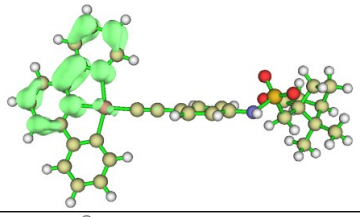
	S4 430 nm f = 0.0133	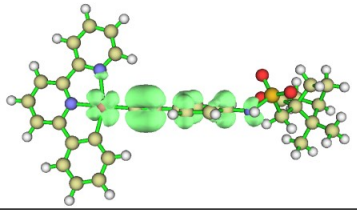	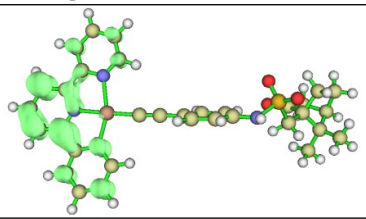
	S8 362 nm f = 0.185	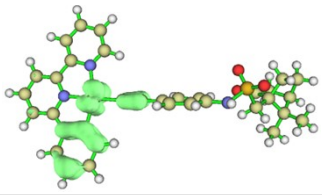	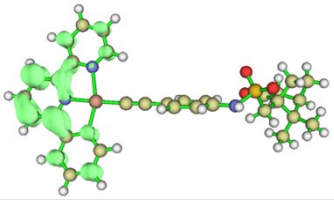
	S9 344 nm f = 0.162	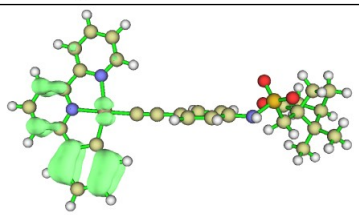	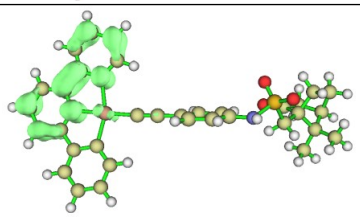
	S13 312 nm f = 0.119	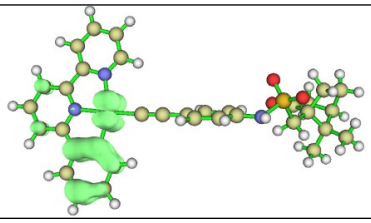	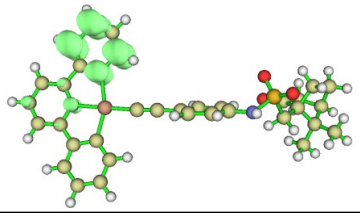

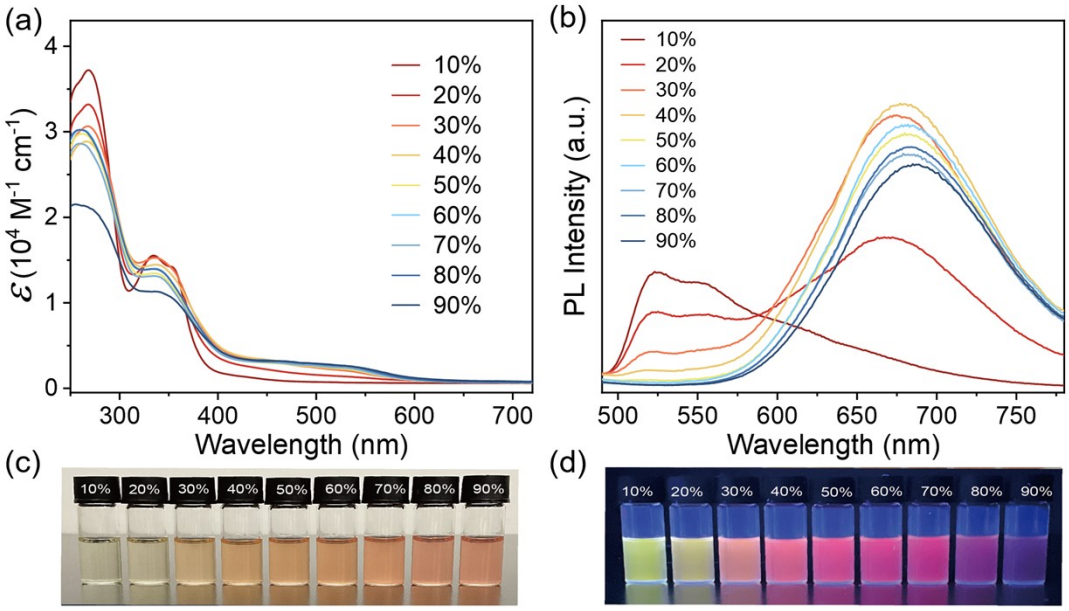

Figure S35. (a) UV-vis and (b) Emission spectra excited at 420 nm of **Pt-2** in versus MCH fraction in the MCH-$CHCl_3$ mixture, and photographs of complex **Pt-2** in the $CHCl_3$-MCH mixture under visible light (c) and 365 nm UV light (d) irradiation.

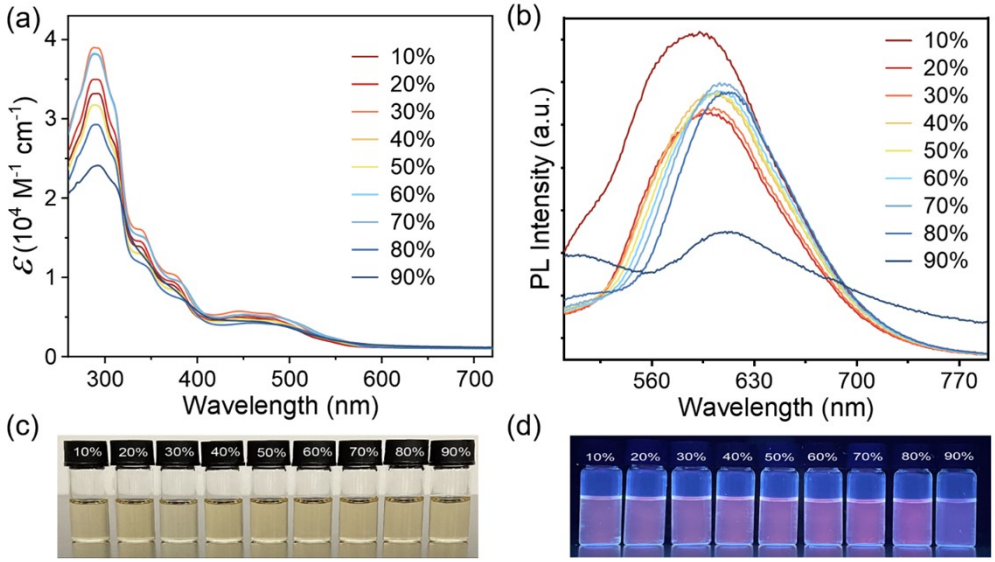

Figure S36. (a) UV-vis and (b) Emission spectra excited at 420 nm of **Pt-3** in versus MCH fraction in the MCH-$CHCl_3$ mixture, and photographs of complex **Pt-3** in the $CHCl_3$-MCH mixture under visible light (c) and 365 nm UV light (d) irradiation.

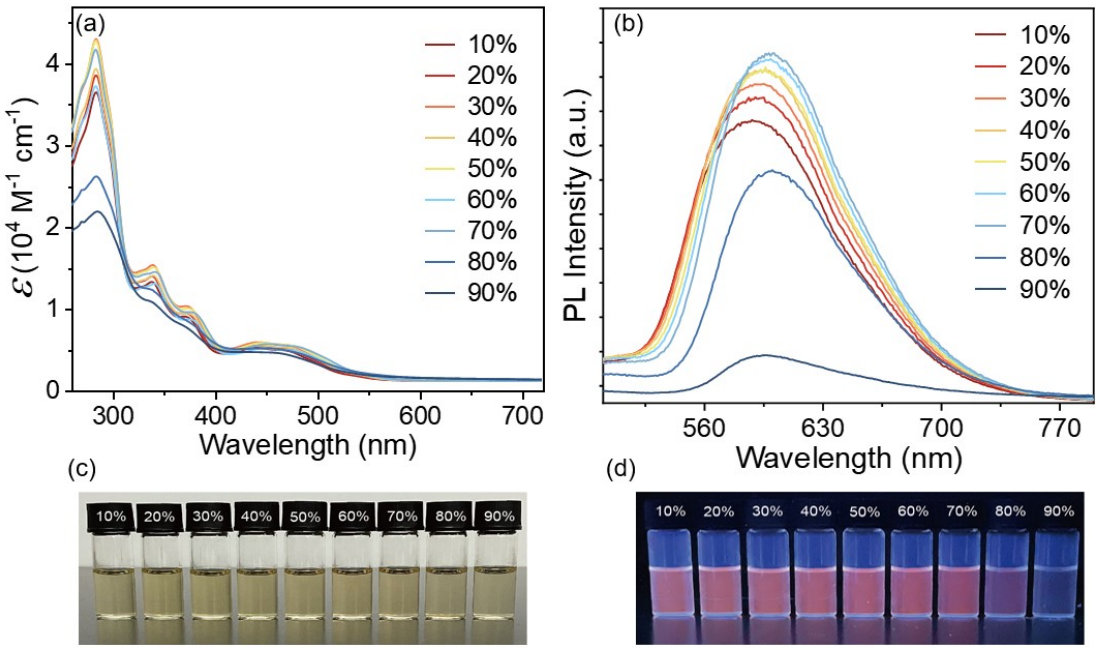

Figure S37. (a) UV-vis and (b) Emission spectra excited at 420 nm of **Pt-4** in the MCH-$CHCl_3$ mixture of versus MCH fraction, and photographs of complex **Pt-4** in the $CHCl_3$-MCH mixture under visible light (c) and 365 nm UV light (d) irradiation.

Table S4. Photophysical and chiroptical data for complexes **Pt-1, Pt-2**, **Pt-3** and **Pt-4**.

Complex	Solution	Electronic absorption λ_{max} /nm (ε/10^4 M^{-1} cm^{-1})	Emission λ_{em}/nm (τ/ns)	QY_{PL}	CPL λ_{em}/nm	g_{lum}
Pt-1	$CHCl_3$	279 (3.98), 333 (1.67), 354 (1.60)	528 (536.7)	0.04	531	1×10^{-4}
	MeCN	276 (4.40), 330 (1.82), 350 (1.83)	528 (337)	0.01		
	PhMe	338 (0.54), 455 (0.10)	660 (479)	0.26		
	$CHCl_3$:MCH [v/v, 6:4]	278 (3.59), 333 (1.54), 354 (1.40)	520(497), 549(464.3), 674 (351.3)	0.06		
	$CHCl_3$:MCH [v/v, 2:8]	276 (2.54), 340 (1.14), 540 (0.25)	689 (228.5)	0.09	710	0.013
Pt-2	$CHCl_3$	269 (4.03), 334 (1.70), 354 (1.58), 415 (0.11)	527 (514.7)	0.04	532	1×10^{-4}
	MeCN	267 (4.19), 330 (1.71), 350 (1.70), 425 (0.08)	524 (328)	0.01		
	PhMe	341 (0.70), 539 (0.13)	683 (289)	0.20		
	$CHCl_3$:MCH [v/v, 6:4]	266 (2.89), 337 (1.45), 542 (0.21)	680 (492)	0.22		
	$CHCl_3$:MCH [v/v, 2:8]	259 (3.02), 339 (1.39), 540 (0.25)	684 (251)	0.14	694	0.023
Pt-3	$CHCl_3$	293 (4.00), 311 (3.22), 339 (1.60), 374 (1.00), 460 (0.48)	601 (60)	0.02		
	MeCN	289 (4.08), 308 (3.15), 330 (1.68), 363 (1.04), 441 (0.56)	604 (23)	0.01		
	PhMe	312 (3.48), 343 (1.50), 382 (0.87), 476 (4.48)	612 (59)	0.02		
	$CHCl_3$:MCH [v/v, 6:4]	288 (3.18), 340 (1.30), 377 (0.84), 448 (0.48), 473 (0.46)	604 (-)	0.01		
	$CHCl_3$:MCH [v/v, 2:8]	290 (2.93), 309 (2.52), 344 (1.15), 385 (0.71), 458 (0.43), 494 (0.40)	611 (50)	0.01		
Pt-4	$CHCl_3$	284 (3.85), 338 (1.32), 370 (0.87), 440 (0.45), 469 (0.41)	592 (66)	0.02		
	MeCN	284 (4.01), 329 (1.40), 361 (0.92), 433 (0.51)	585 (76)	0.01		
	PhMe	344 (1.31), 383 (0.79), 459 (0.44), 483 (0.43)	601 (-)	0.02		
	$CHCl_3$:MCH [v/v, 6:4]	284 (3.93), 340 (1.39), 374 (0.93), 445 (0.54), 473 (0.51)	600 (-)	0.02		
	$CHCl_3$:MCH [v/v, 2:8]	284 (2.61), 339 (1.22), 376 (0.82), 456 (0.50)	602 (-)	0.01		

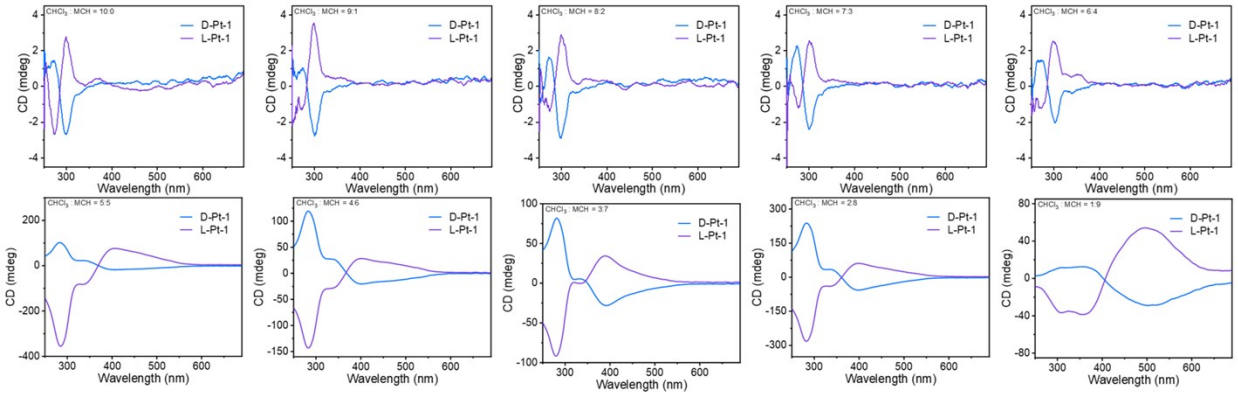

Figure S38. CD spectra of **D/L-Pt-1** in the MCH-$CHCl_3$ mixture of versus MCH fraction.

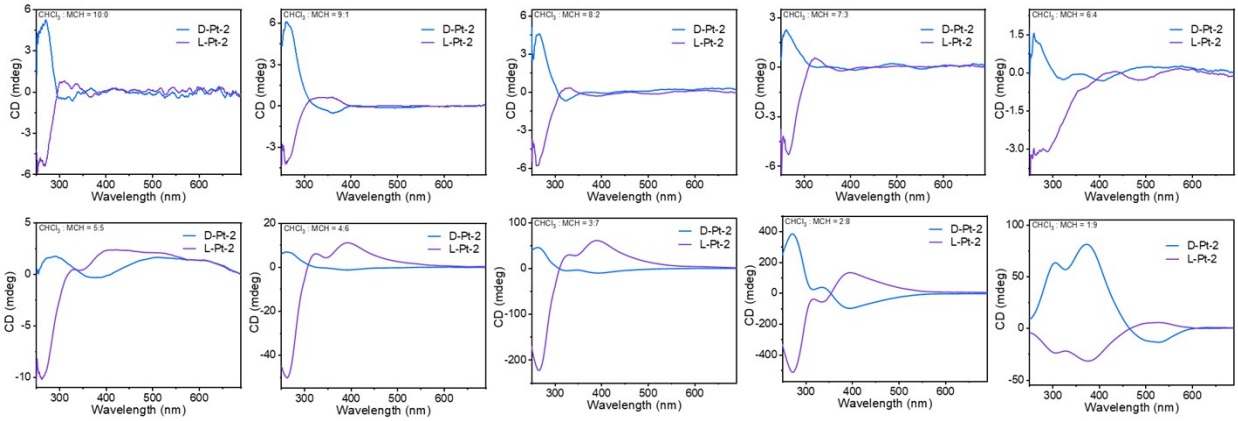

Figure S39. CD spectra of **D/L-Pt-2** in the MCH-$CHCl_3$ mixture of versus MCH fraction.

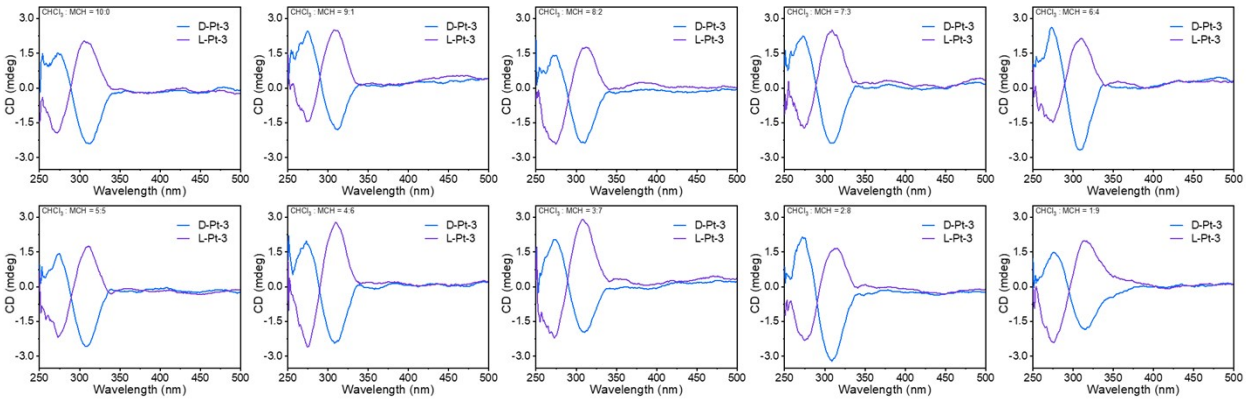

Figure S40. CD spectra of **D/L-Pt-3** in the MCH-$CHCl_3$ mixture of versus MCH fraction.

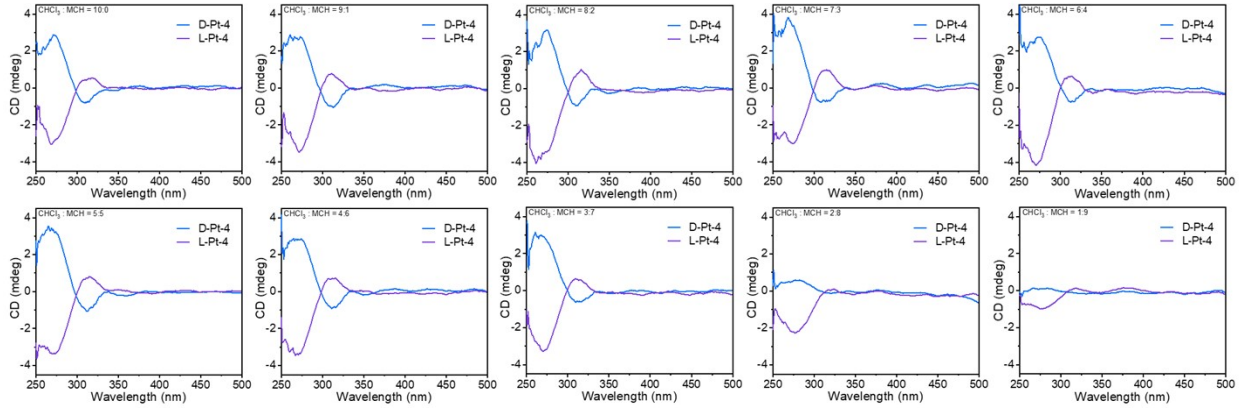

Figure S41. CD spectra of **D/L-Pt-4** in the MCH-$CHCl_3$ mixture of versus MCH fraction.

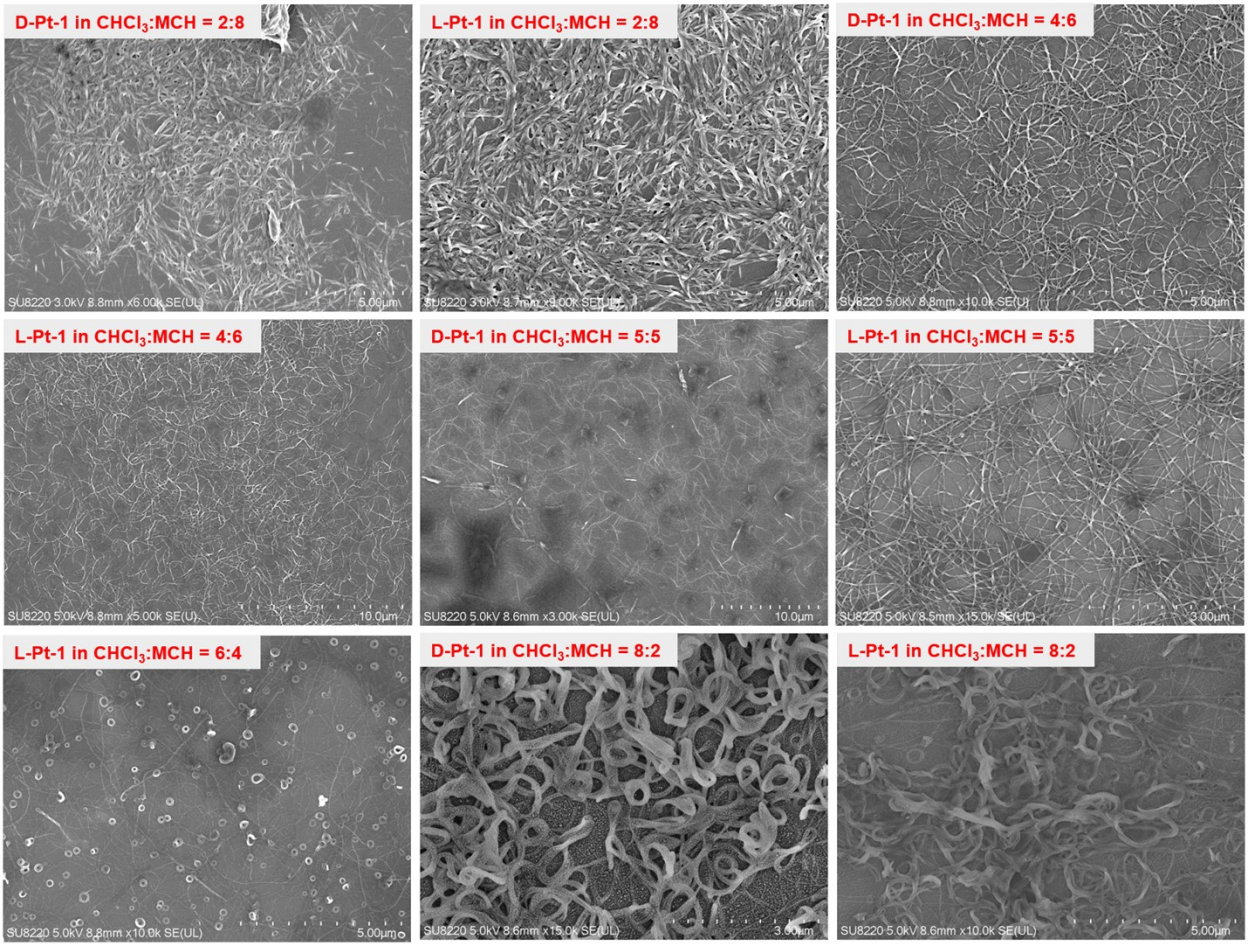

Figure S42. SEM images of **D/L-Pt-1** self-assemblies prepared in MCH-$CHCl_3$ with different MCH ratio at R.T. without aging.

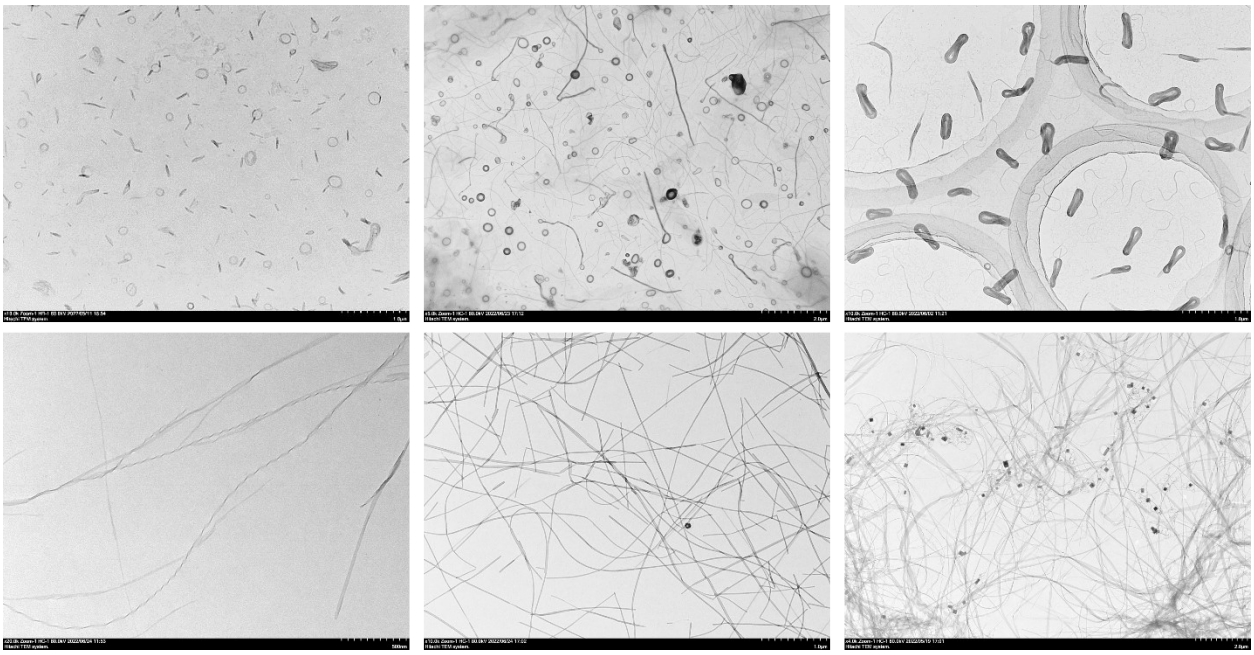

Figure S43. Representative TEM images for **L-Pt-1** self-assemblies prepared in MCH-$CHCl_3$.

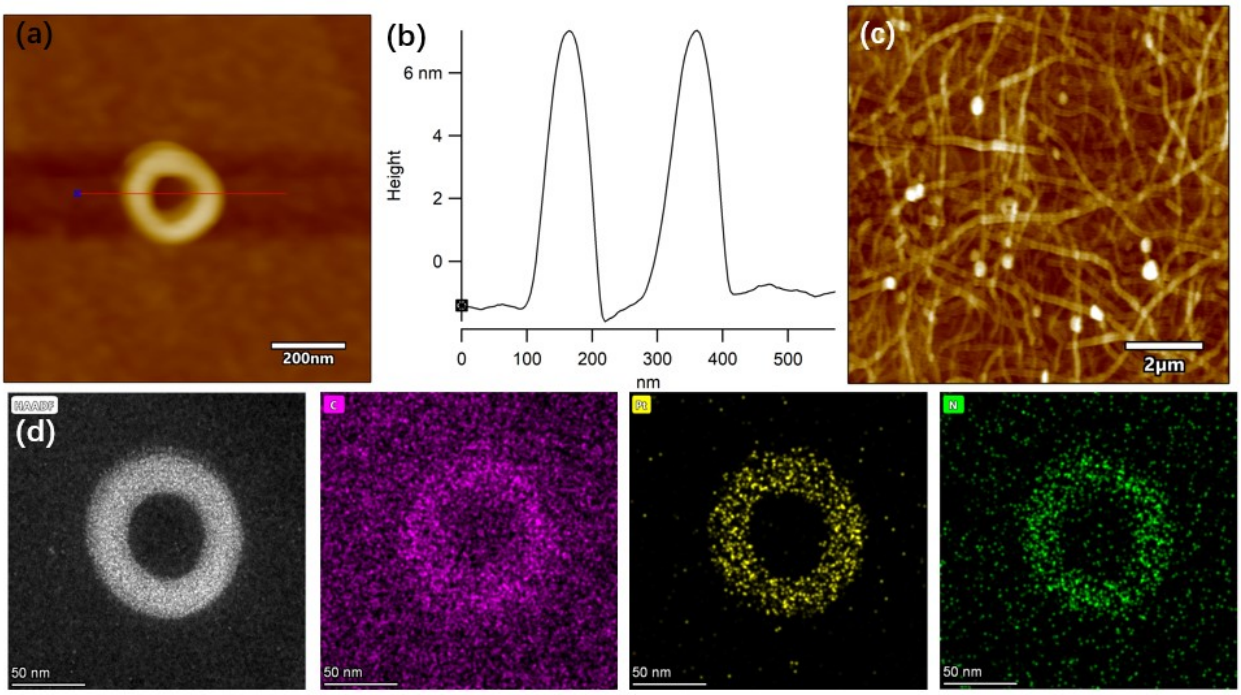

Figure S44. AFM images of **L-Pt-1** self-assemblies prepared in 40% MCH- $CHCl_3$ solution (a) at R.T. without aging, and (c) after aging for 6 h at 288 K. (b) Height profile of the nanoring at the selected cross-section. (d) The HAADF-STEM image and corresponding EDS mapping of **L-Pt-1** self-assemblies.

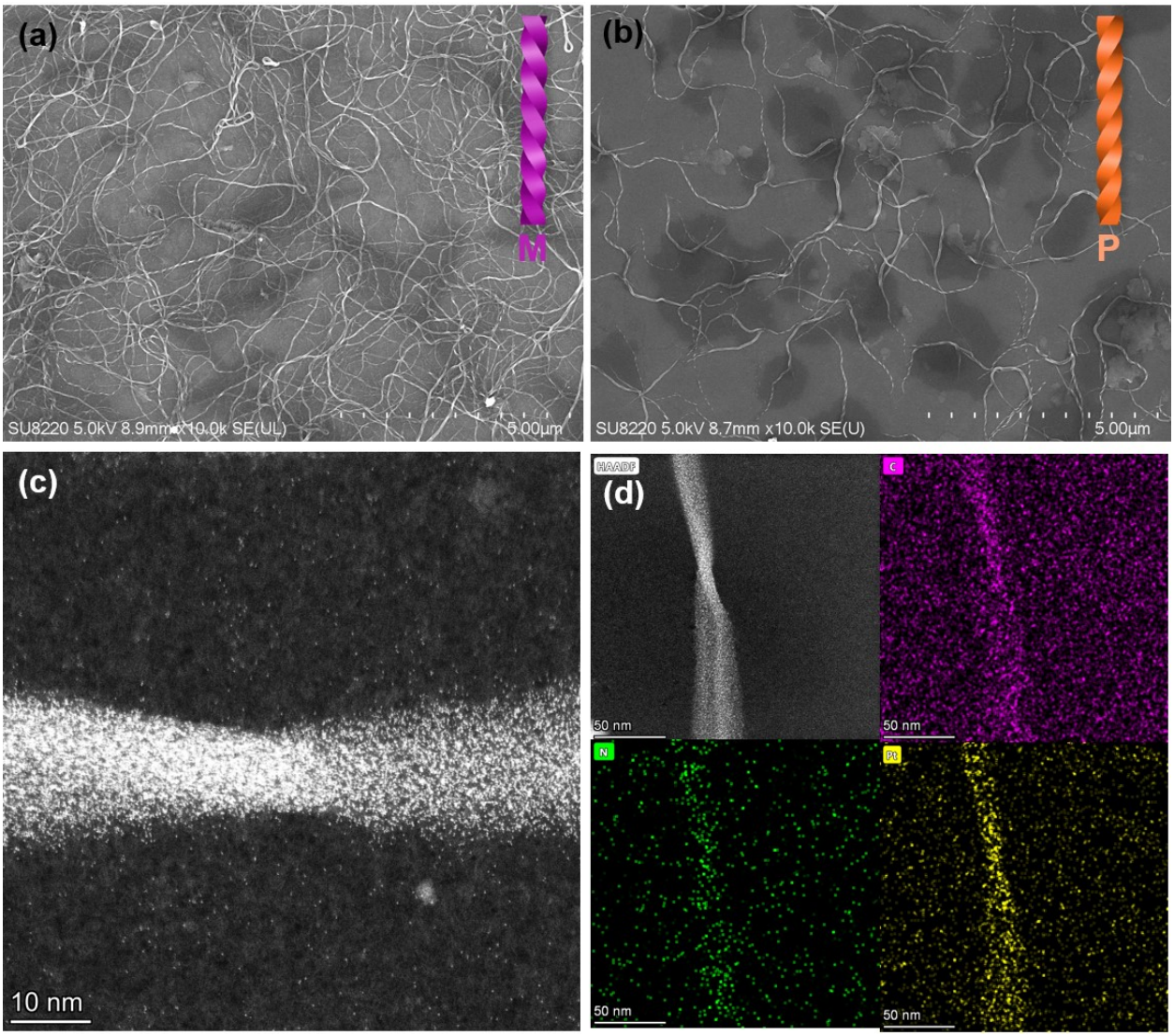

Figure S45. (a) SEM images of **D-Pt-1**, (b) **L-Pt-1**, (c) HAADF-STEM image and (d) corresponding EDS mapping of **D-Pt-1** self-assemblies prepared in MCH-$CHCl_3$ with 40% MCH ratio after aging for 6 h at 288 K.

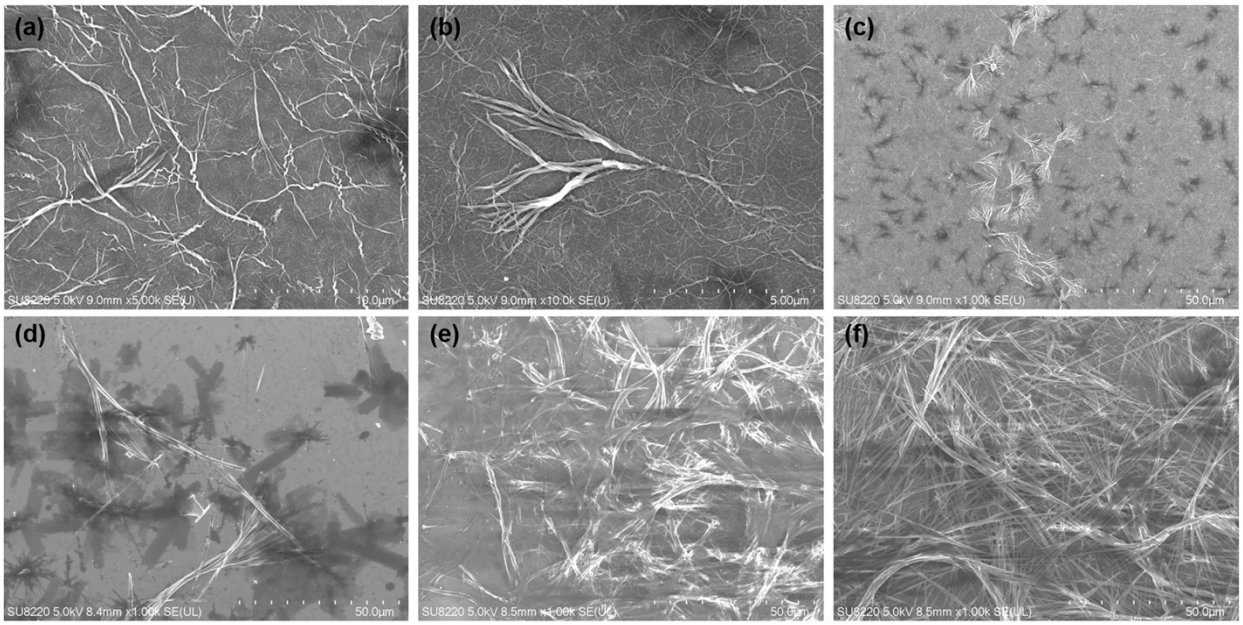

Figure S46. SEM images of **D-Pt-1** self-assemblies dendritic nanotwists prepared in 40% MCH-$CHCl_3$ solution after aging for 12 h (a-c) at 288 K; (d-f) prolong the aging time at R.T.

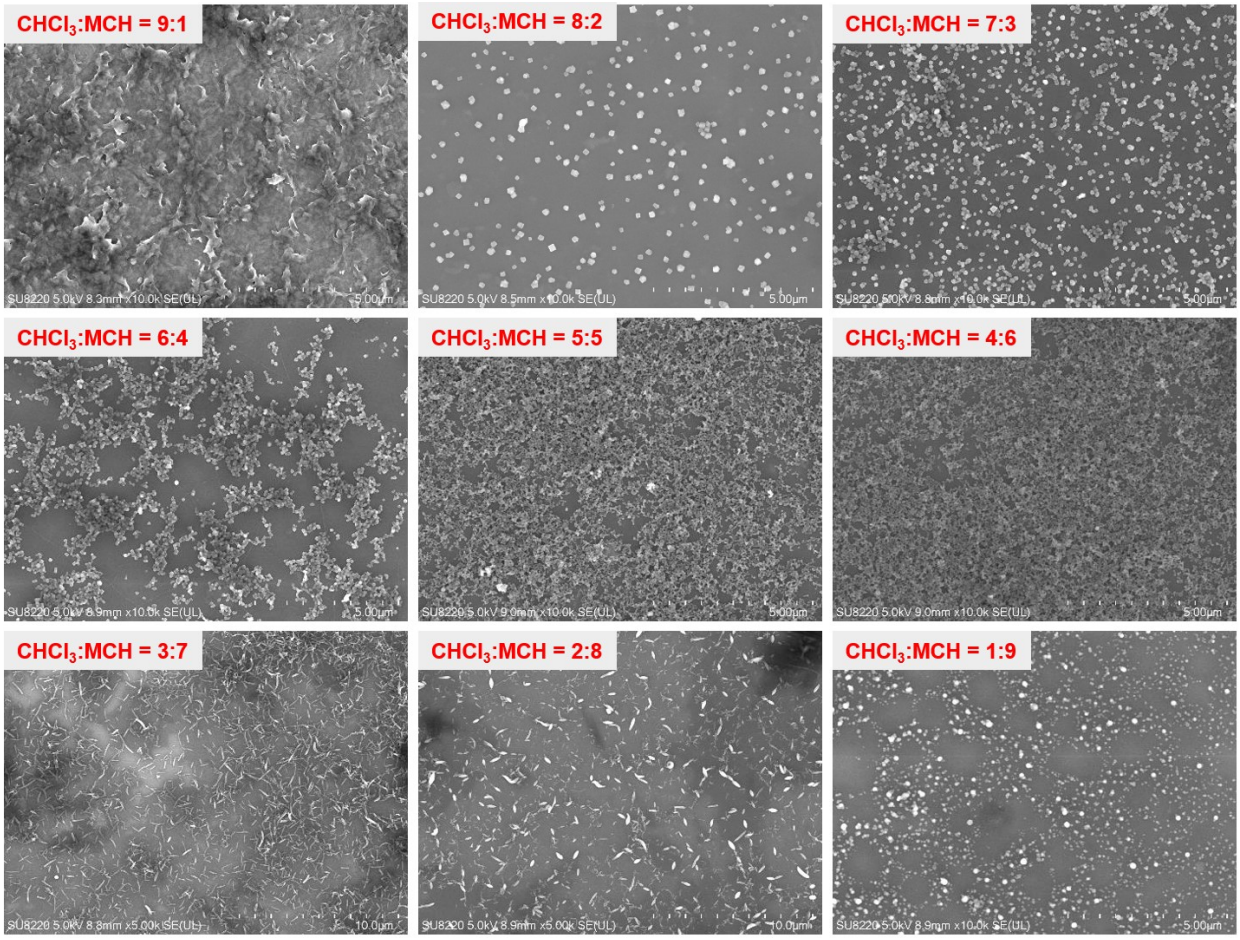

Figure S47. SEM images of **L-Pt-2** self-assemblies prepared in MCH-$CHCl_3$ with different MCH ratio without aging. No obvious difference was observed for the SEM images of **D-Pt-2**.

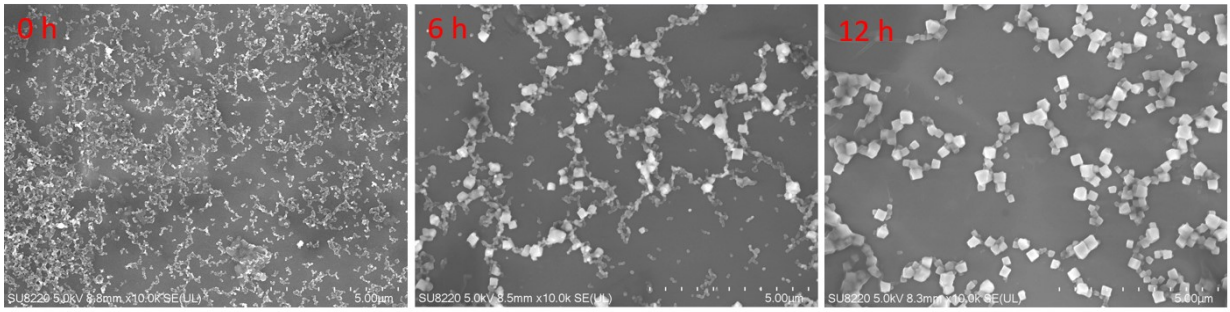

Figure S48. SEM images of **L-Pt-2** self-assemblies prepared in MCH-$CHCl_3$ with 40% MCH after various aging for a certain time.

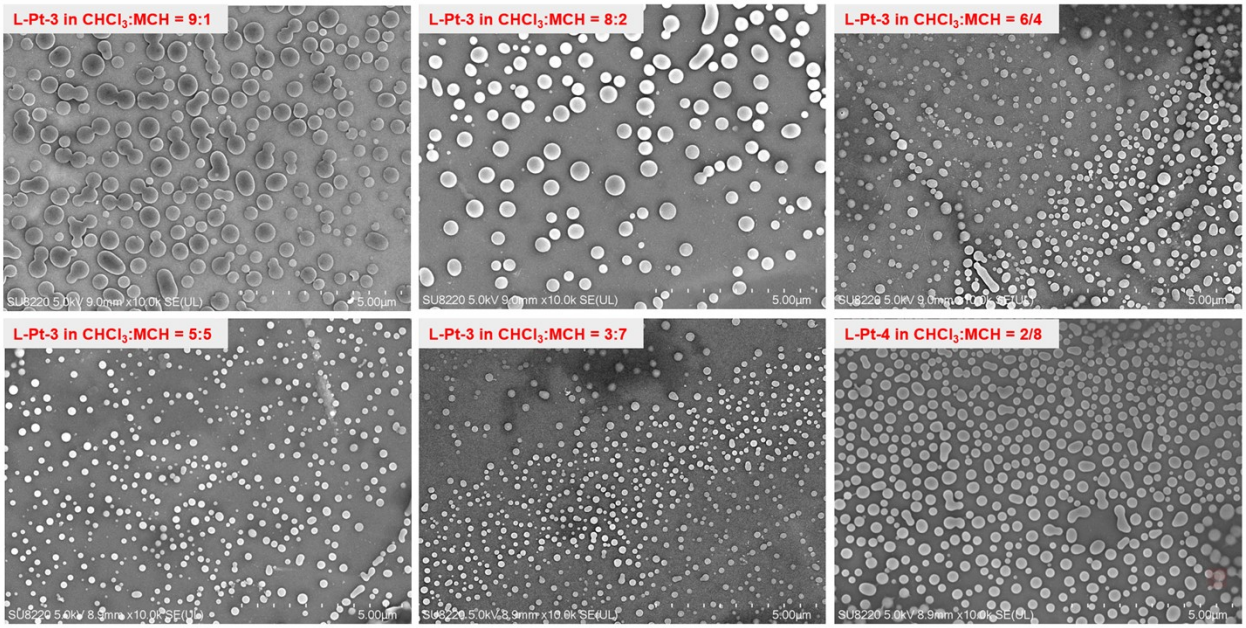

Figure S49. SEM images of **L-Pt-3** self-assemblies prepared in MCH-$CHCl_3$ with different MCH ratio.

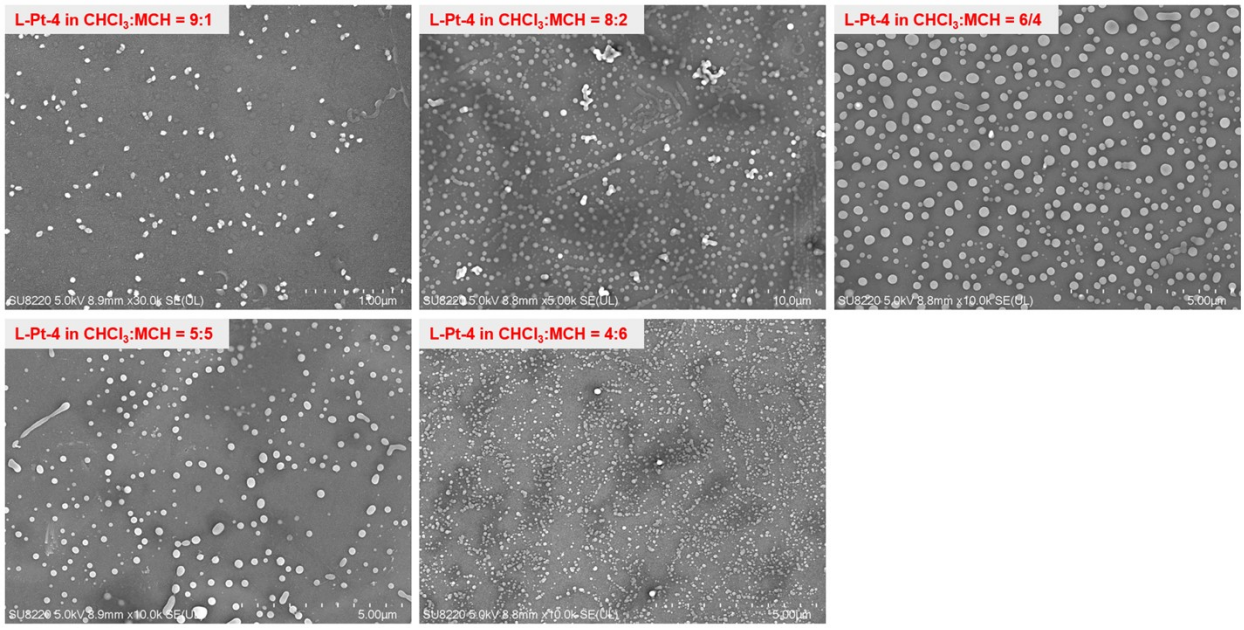

Figure S50. SEM images of **L-Pt-4** self-assemblies prepared in MCH-$CHCl_3$ with different MCH ratio.

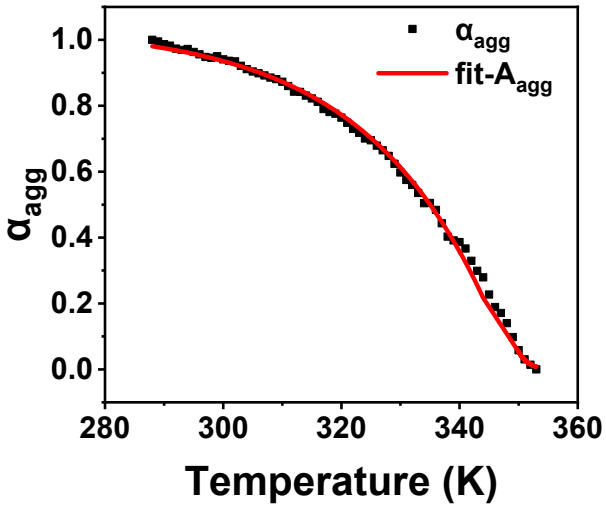

Table S5. Thermodynamic parameters describing the self-assembly of **Pt-1** in TCE/MCH (v/v, 3/7, c = 50 μM) at different temperature.

K_n	K_e	σ	ΔH (kJ/mol)	ΔS (J/mol·K)	ΔG (kJ/mol)
9.94×10^{-4}	17.35	1.20×10^{-3}	-39.59	-112.87	-7.08

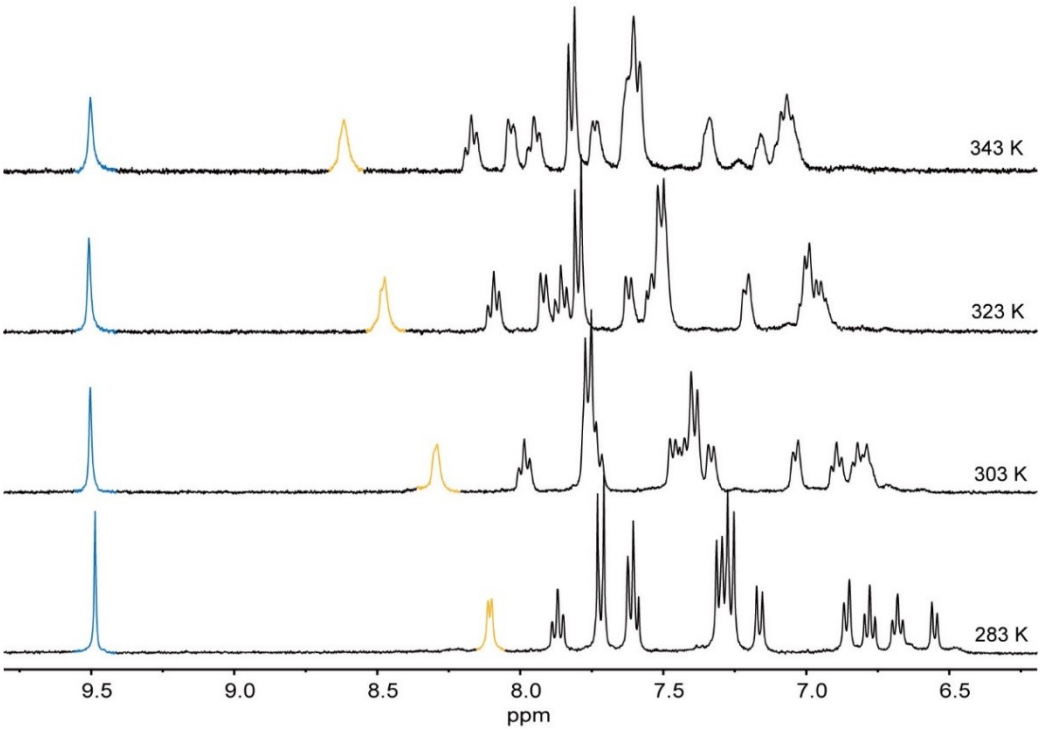

Figure S51. Temperature-dependent ^{1}H NMR spectra of **Pt-1** in CD_3CN.

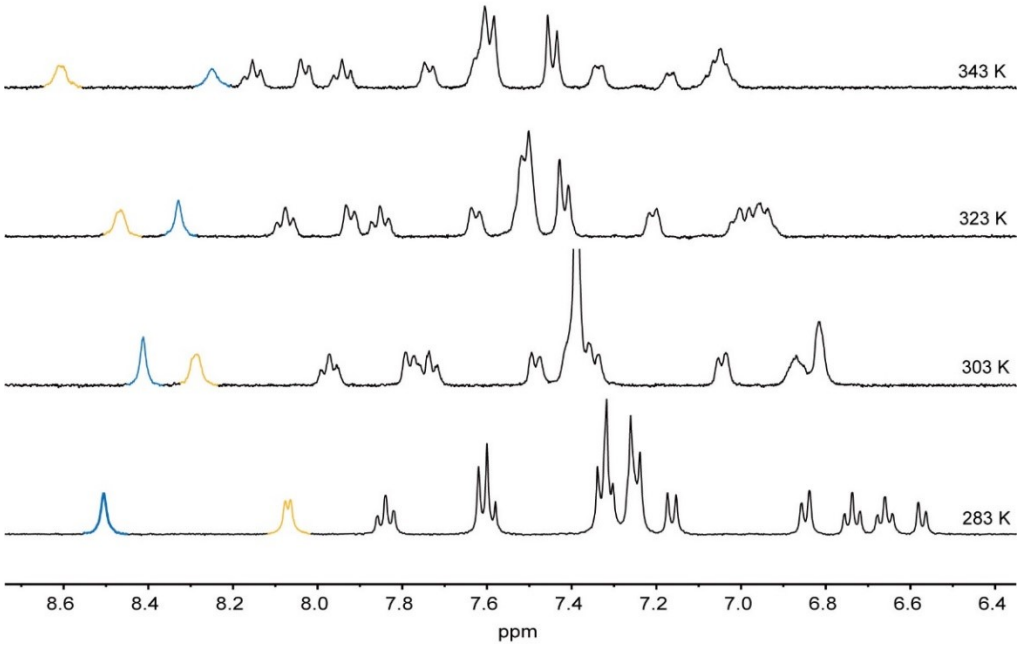

Figure S52. Temperature-dependent ^{1}H NMR spectra of **Pt-2** in CD_3CN.

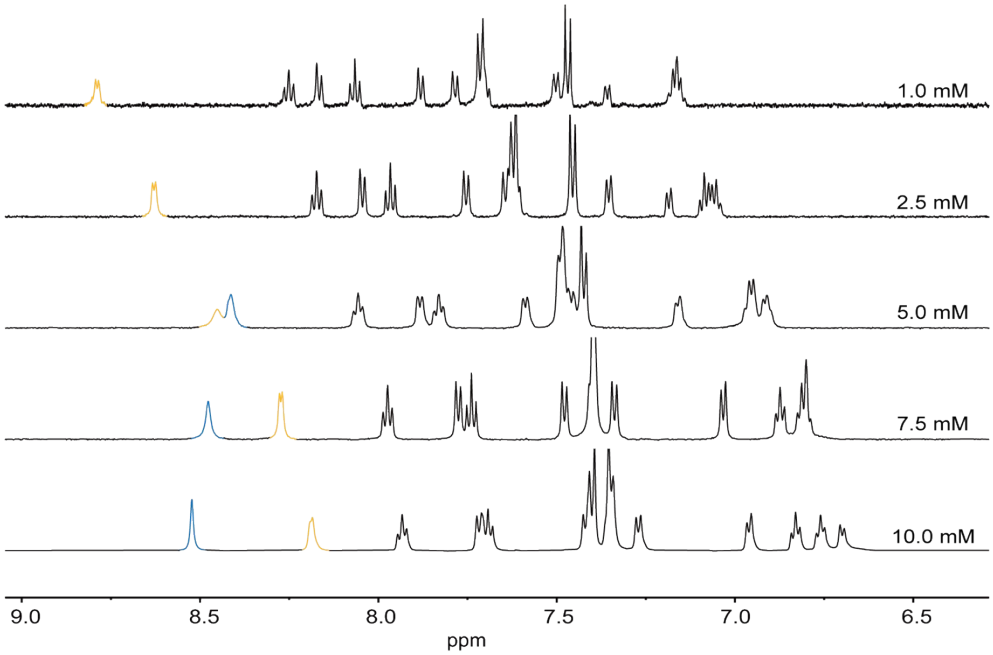

Figure S53. Concentration-dependent ^{1}H NMR spectra of **Pt-2** in $CDCl_3$ at 298 K.

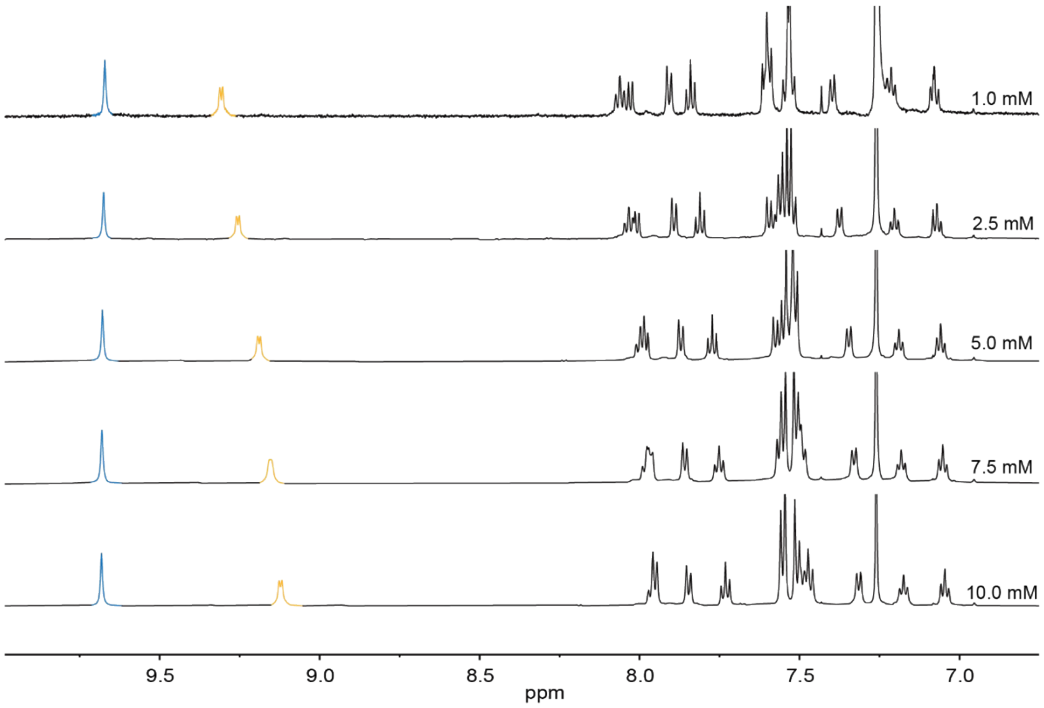

Figure S54. Concentration-dependent ^{1}H NMR spectra of **Pt-3** in $CDCl_3$ at 298 K.

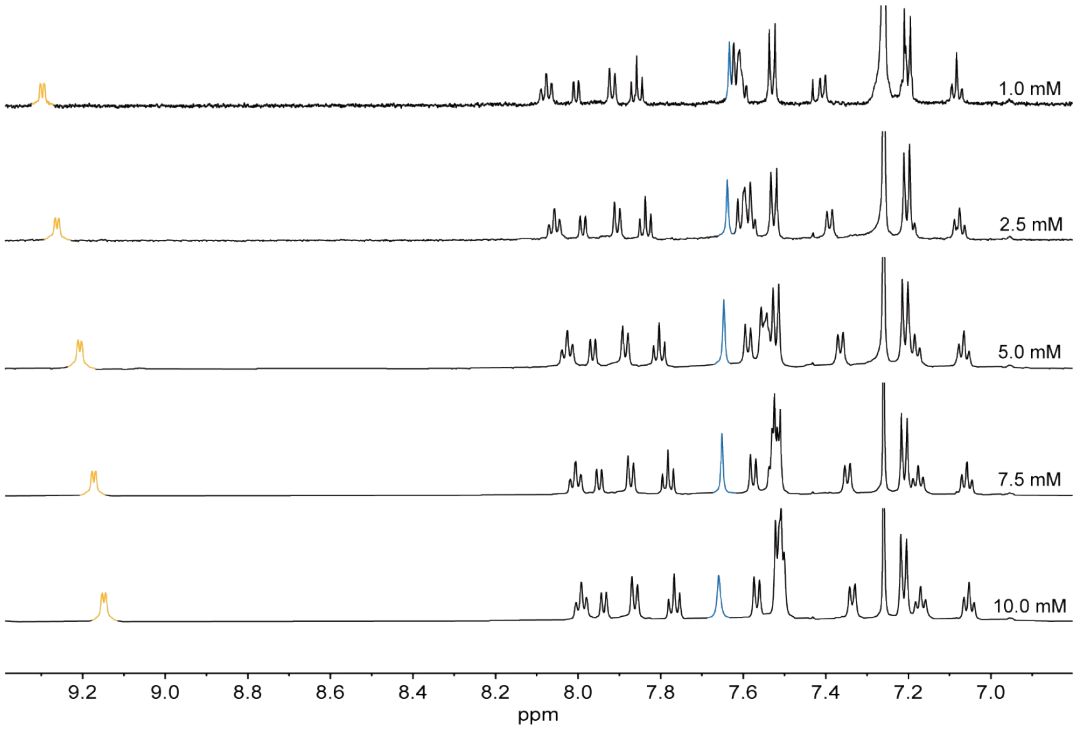

Figure S55. Concentration-dependent ^{1}H NMR spectra of **Pt-4** in $CDCl_3$ at 298 K.

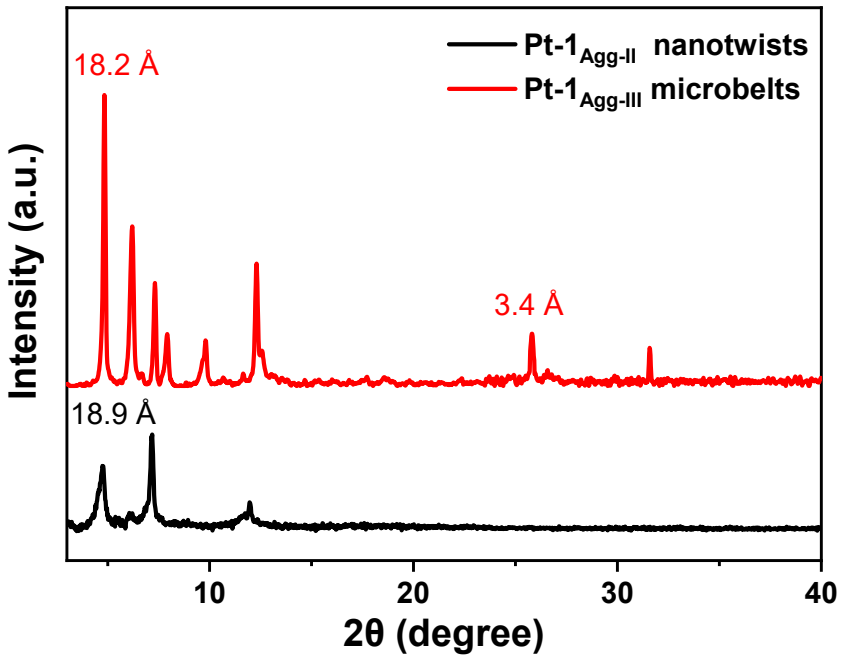

Figure S56. PXRD patterns of nanotwist and microbelt assemblies for **Pt-1**.

The powder X-ray diffraction (PXRD) patterns of **Pt-1** display relatively high crystallinity for nanotwist and microbelt structures (Fig. S56). Based on Bragg's equation, the d spacing changed into 1.89 and 1.82 nm for the nanotwists and microbelts, respectively. Based on the DFT calculation, the molecular length of **Pt-1** was estimated to be 2.01 nm. A slightly smaller d value as compared to the extended molecular length is assignable to monolayer structure.[5] The changes of these reflections indicate that the d spacing are slightly compressed from nanotwists to form microbelts.

Reference:

1. K. Heinze and V. Jacob, *Eur. J. Inorg. Chem.*, 2003, **2003**, 3918-3923.
2. W. Lu, V. A. Roy and C.-M. Che, *Chem. Commun.*, 2006, 3972-3974.
3. K. M.-C. Wong, W.-S. Tang, X.-X. Lu, N. Zhu and V. W.-W. Yam, *Inorg. Chem.*, 2005, **44**, 1492-1498.
4. U. Huynh, S. L. McDonald, D. Lim, M. N. Uddin, S. E. Wengryniuk, S. Dey and D. M. Coltart, *J. Org. Chem.*, 2018, **83**, 12951-12964.
5. N. Kameta, M. Masuda, H. Minamikawa, T. Shimizu, *Langmuir*, 2007, **23**, 4634-4641.